Bioorganic & Medicinal Chemistry 17 (2009) 7368–7380

Contents lists available at ScienceDirect

Bioorganic & Medicinal Chemistry

journal homepage: www.elsevier.com/locate/bmc

Glucose-based spiro-isoxazolines: A new family of potent glycogen phosphorylase inhibitors

Mahmoud Benltifa [a,b,c,d], Joseph M. Hayes [e], Sébastien Vidal [a,b,c,d], David Gueyrard [a,b,c,d], Peter G. Goekjian [a,b,c,d], Jean-Pierre Praly [a,b,c,d,*], Gregory Kizilis [e], Costas Tiraidis [e], Kyra-Melinda Alexacou [e], Evangelia D. Chrysina [e,*], Spyros E. Zographos [e], Demetres D. Leonidas [e], Georgios Archontis [f], Nikos G. Oikonomakos [e,†]

[a] Université de Lyon, Institut de Chimie et Biochimie Moléculaires et Supramoléculaires associé au CNRS, UMR 5246, Laboratoire de Chimie Organique 2, Bâtiment Curien, 43 Boulevard du 11 Novembre 1918, F-69622 Villeurbanne, France
[b] Université Lyon 1, F-69622 Villeurbanne, France
[c] CNRS, UMR5246, Institut de Chimie et Biochimie Moléculaires et Supramoléculaires (ICBMS), Laboratoire de Chimie Organique 2, Bâtiment Curien, 43 Boulevard du 11 Novembre 1918, F-69622 Villeurbanne, France
[d] CPE-Lyon, F-69616 Villeurbanne, France
[e] Institute of Organic and Pharmaceutical Chemistry, National Hellenic Research Foundation, 48 Vassileos Constantinou Avenue, Athens 11635, Greece
[f] Department of Physics, University of Cyprus, PO Box 20537, CY1678 Nicosia, Cyprus

ARTICLE INFO

Article history:
Received 25 March 2009
Revised 6 August 2009
Accepted 11 August 2009
Available online 2 September 2009

Keywords:
Glycogen phosphorylase
1,3-Dipolar cycloaddition
Isoxazoline
X-ray crystallography
GLIDE docking calculations
Quantum polarized ligand docking (QPLD)

ABSTRACT

A series of glucopyranosylidene-spiro-isoxazolines was prepared through regio- and stereoselective [3+2]-cycloaddition between the methylene acetylated *exo*-glucal and aromatic nitrile oxides. The deprotected cycloadducts were evaluated as inhibitors of muscle glycogen phosphorylase b. The carbohydrate-based family of five inhibitors displays K_i values ranging from 0.63 to 92.5 μM. The X-ray structures of the enzyme–ligand complexes show that the inhibitors bind preferentially at the catalytic site of the enzyme retaining the less active T-state conformation. Docking calculations with GLIDE in extra-precision (XP) mode yielded excellent agreement with experiment, as judged by comparison of the predicted binding modes of the five ligands with the crystallographic conformations and the good correlation between the docking scores and the experimental free binding energies. Use of docking constraints on the well-defined positions of the glucopyranose moiety in the catalytic site and redocking of GLIDE-XP poses using electrostatic potential fit-determined ligand partial charges in quantum polarized ligand docking (QPLD) produced the best results in this regard.

1. Introduction

Type 2 diabetes is characterized by hyperglycemia resulting from defects in insulin secretion, insulin action or both.[1] The chronic hyperglycemia of diabetes is associated with long-term damage, dysfunction, and failure of various organs, especially the eyes, kidneys, nerves, heart, and blood vessels.[2] Glycogen phosphorylase (GP) catalyzes the breakdown of glycogen to glucose-1-phosphate in the liver and in tissues fluctuating with energy demands.[3,4] Two interconvertible forms of GP exist: GPa refers to the phosphorylated form (high activity, high substrate affinity, predominantly relaxed (R) state), and GPb is the non-phosphorylated enzyme (low activity, low substrate affinity, predominantly tense (T) state). Among the different therapeutic targets for the treatment of type 2 diabetes, the design of inhibitors of GP is a promising therapeutic strategy with potential pharmaceutical applications in improving glycemic control in type 2 diabetes.[5]

Several inhibitors of GP have been reported in the literature[6–9] and the glucose-based ones[6,7] were shown to bind selectively at the catalytic site of this enzyme (either GPa or GPb) in contrast with other families of inhibitors interacting at other sites. Glucopyranosylidene-spiro-heterocycles **A**–**L** (Fig. 1) display interesting inhibitory activities in which glucopyranosylidene-spiro-hydantoin **A** appears as the most effective glucose analogue inhibitor. Crystallographic studies[10] of the GPb–**A** complex have shown that **A** binds at the catalytic site mainly through a dense hydrogen bond network. Most of these analogues exploit the formation of hydrogen bonds with the amino-acids of GP's catalytic site and the changes in inhibition are mostly related to a varying number of

* Corresponding authors. Tel.: +33 472 43 11 61; fax: +33 478 89 89 14 (J.-P. P.); tel.: +30 210 7273851; fax: +30 210 7273831 (E.D.C.).
E-mail addresses: jean-pierre.praly@univ-lyon1.fr (J.-P. Praly), echrysina@eie.gr (E.D. Chrysina).
† Dr. Nikos G. Oikonomakos sadly passed away on the 31st of August 2008 during the preparation of this manuscript. This paper is dedicated to his memory.

0968-0896/$ - see front matter © 2009 Elsevier Ltd. All rights reserved.
doi:10.1016/j.bmc.2009.08.060

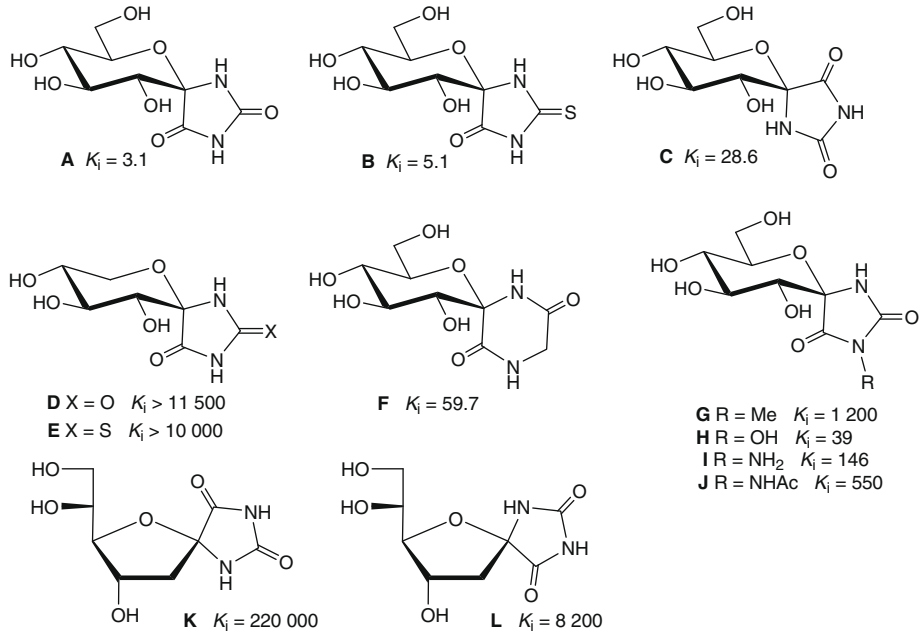

Figure 1. Representative glucopyranosylidene-spiro-heterocyclic inhibitors of rabbit muscle GPb and their K_i (μM).[6,7]

possible interactions. Nevertheless, none of these inhibitors occupy the so-called β-pocket in close vicinity to the catalytic site, which is lined by both polar and nonpolar groups and has no access to the bulk solvent.[11]

We have previously reported the synthesis of a series of gluco-[12] and galactopyranosylidene-spiro-oxathiazoles[13] incorporating an aromatic moiety at the 3-position of the oxathiazole ring (Fig. 2). Preliminary results showed that glucose-based 3-phenyl oxathiazole derivatives inhibited GPb with K_i values of 25.9 μM (R = H) and 48.0 μM (R = *p*-F).[14] We therefore recently performed the synthesis of a family of glucopyranosylidene-spiro-oxathiazoles and also studied the inhibition of glycogen phosphorylase.[15] Glucopyranosylidene-spiro-isoxazolines have attracted our attention as a novel class of inhibitors of GP.[16] They were presumed to preserve the main structural features of glucose-based GP inhibitors such as the $^4C_1$ ring conformation, with the oxygen and nitrogen atoms in the heterocyclic ring available to hydrogen bonding with amino-acids. An important feature of the new compounds is the presence of aromatic groups that occupy the β-pocket in the enzyme.

Five new glucopyranosylidene-spiro-isoxazolines were synthesized and tested for their inhibitory effect on GPb upon binding by kinetic assays and X-ray crystallographic experiments. The K_i values obtained varied from 0.63 to 92.5 μM for the new analogues. All the inhibitors bind at the catalytic site of the enzyme which retains its less active T-state conformation.

In earlier work, we demonstrated that GLIDE[17,18] docking calculations could successfully reproduce the binding of glucose-based inhibitors at the catalytic site of GP.[19] With the aim to develop a new computational protocol that can accurately predict experimental binding properties, in the current work we have performed molecular modeling studies of the GP–spiro-isoxazoline complexes, using GLIDE and quantum polarized ligand docking[20] (QPLD) from calculations in extra-precision (XP) mode. The importance of more accurate charges derived using quantum mechanics (QM) or hybrid quantum mechanics/molecular mechanics (QM/MM) methods has recently been highlighted.[21,22] We compare the docking results of QPLD-XP calculations with optimized electrostatic potential (ESP) ligand atomic charges, to results obtained by standard GLIDE-XP calculations with OPLS-AA(2001) forcefield[23] ligand atomic charges. For the QPLD-XP runs, the top-ranked poses from the standard GLIDE-XP calculations were subjected to reassignment of ligand partial charges. This was done by fitting to ESPs generated by single point energy calculations on the ligand binding poses either in the free state, using QM (free ligand; no receptor), or in the 'field' of the receptor using QM/MM, accounting for receptor–ligand charge polarization effects. The ligand poses with the new partial charges were then redocked

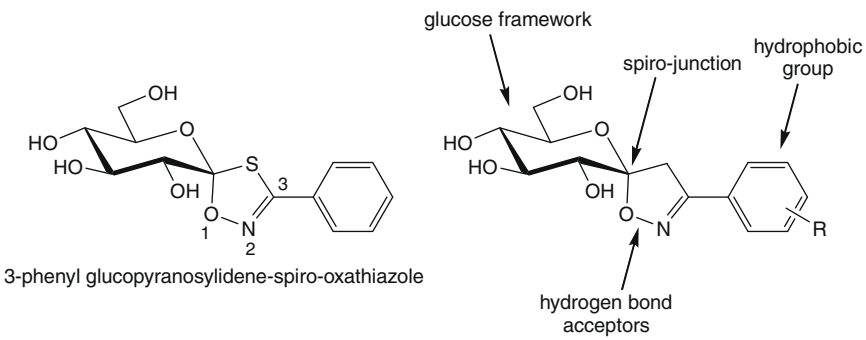

Figure 2. Structure of 3-aryl glucopyranosylidene-spiro-oxathiazoles and expected interactions associated with the glucopyranosylidene-spiro-isoxazoline inhibitors.

into the receptor using GLIDE-XP. We also investigated the effect on accuracy due to introducing positional constraints on parts of the ligand. The quality of generated docking conformations was expected to be strongly correlated with scoring.[24–26] In this work, the best results were obtained using QPLD-XP with electrostatic potential (ESP) fit-determined ligand partial charges calculated in the 'field' of the receptor with constraints on the well-defined glucopyranose moiety atomic positions. An average RMSD (heavy atoms) between superimposed crystallographic and top-ranked ligand docking conformations of 0.691 Å was obtained using this method, with an impressive correlation (R^2 = 0.958) between the docking GlideScores (GSs) and experimental binding free energies. Overall, the results obtained were in excellent agreement with those from kinetic and crystallographic studies both in terms of experimental free binding energy and mode of binding for all five ligands.

2. Results and discussion

2.1. Synthesis of glucopyranosylidene-spiro-isoxazolines

Although [3+2]-cycloaddition reactions[27] have been applied to carbohydrates for a long time,[28] their synthetic potential for preparing heterocycles by regio- and stereoselective formation of covalent bonds with atom economy recently arise strong interest. For example, sugar-based dipoles such as glycosyl azides,[29–31] nitrile oxides[32] or nitrones[32] have permitted significant advances. Unsaturated sugars and in particular *exo*-glycals[33,34] proved to be useful as dipolarophiles. Although the regio- and stereoselectivities of these reactions have been well documented in the literature, none of these studies reported the final deprotection or biological evaluation of the cycloadducts.

We first designed an approach using benzyl protected *exo*-glycals which provided the desired cycloadducts in good yields. However, the subsequent hydrogenolysis of benzyl ethers was not compatible with the stability of the isoxazoline ring in which the N–O bond was reduced by dihydrogen in the presence of a Pd catalyst, thereby changing drastically the structure of the molecule.[16] We therefore considered acetates as protecting groups for their final removal without altering the spiro-bicyclic system created during the cycloaddition reaction. The previously reported persilylated *exo*-glucal **1**[35] was prepared using our recently reported methodology[36,37] and then converted into the acetylated *exo*-glucal **2**[38,39] in a one-pot procedure (Scheme 1). 1,3-Dipolar cycloadditions with a series of aromatic nitrile oxides, generated in situ from the corresponding hydroximoyl chlorides and triethylamine, afforded cycloadducts **3a–e** in high yields. The regiochemistry of the cycloaddition reaction was demonstrated through a set of NMR experiments (^{1}H, ^{13}C, COSY, HSQC, and HMBC), showing in particular a signal resonating between 106 and 108 ppm in the ^{13}C NMR spectrum corresponding to the anomeric carbon atom for the desired regioisomer.[16] The (*R*) configuration at the anomeric center of **3a–e** was established by NOE experiments which showed consistently a contact between the methylene protons of the isoxazoline ring and the H-2 proton of the sugar ring. This observation demonstrates that the nitrile oxide is approaching the acetylated *exo*-glycal from the bottom α-face, as already observed by other groups. The acetylated cycloadducts were then deprotected under Zemplén conditions to afford the hydroxylated derivatives **4a–e** in nearly quantitative yields.

2.2. Enzyme kinetics

Inhibition constants (K_i) were measured against GPb for compounds **4a–e** (Fig. 3). Structure **4d** with an aromatic ring bearing a *para*-nitro group exhibited a drastically increased K_i value (92.5 μM) in contrast with electron rich, less bulky but more flexible molecules and in particular **4a** (6.6 μM). Interestingly, the presence in **4e** of a hydrophobic extended aromatic system such as a 2-naphthyl moiety improved the K_i value to the sub-μM range. This value was among the lowest reported to date for the glucose-based family of GPb inhibitors.[6,7] The favorable influence of a properly oriented 2-naphthyl residue on binding to the enzyme has been already observed for spiro-compounds,[14,15] *C*-glucosyl heterocycles[40,41] and *N*-glucosyl-*N*′-acyl ureas.[6,7] In order to rationalize the inhibitory activities of **4a–e** on an accurate structural basis, crystallographic studies and docking calculations have been carried out.

2.3. X-ray crystallographic studies

The overall architecture of the native T-state GPb with the location of the catalytic site is shown in Figure 4. Electron density difference maps (Fig. 5) clearly defined the position of each inhibitor within the catalytic site, consistent with the kinetic results. The mode of binding and the interactions that the glucopyranose moiety makes with GPb, in all five inhibitors, is almost identical with those previously described at 100 K from a 1.93 Å resolution crystallographic experiment,[19] except that the atomic positions of C1–C6 and O5 of β-D-glucopyranose are slightly changed in the GPb/**4a–e** structures (compared to those of α-D-glucose) and exhibit shifts of ~0.3–0.5 Å towards the β-pocket. All the inhibitors bound at the catalytic site of the enzyme, by making direct and water-mediated hydrogen bonds with the protein residues and, with

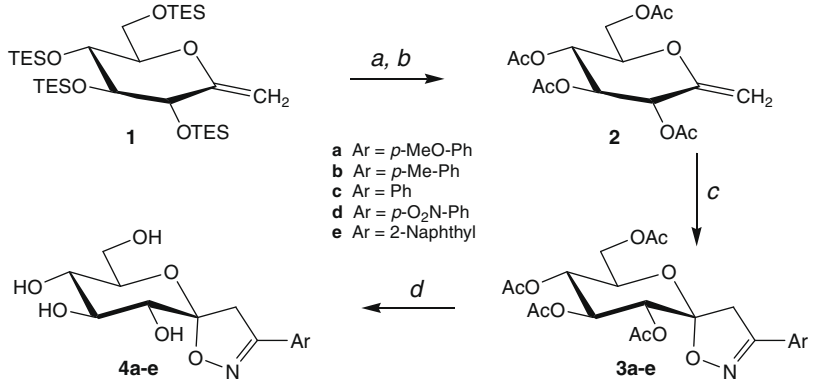

Scheme 1. Preparation of the glucopyranosylidene-spiro-isoxazoline inhibitors **4a–e**. Reagents and conditions: (a) *n*Bu$_4$NF, THF, rt, 4 h; (b) C_5H_5N, Ac_2O, rt, 16 h (87% overall); (c) ArC(Cl)=NOH, Et_3N, CH_2Cl_2, rt, 16 h (83–99%); (d) NaOMe, MeOH, rt, 3 h (78–99%). (TES = Et_3Si).

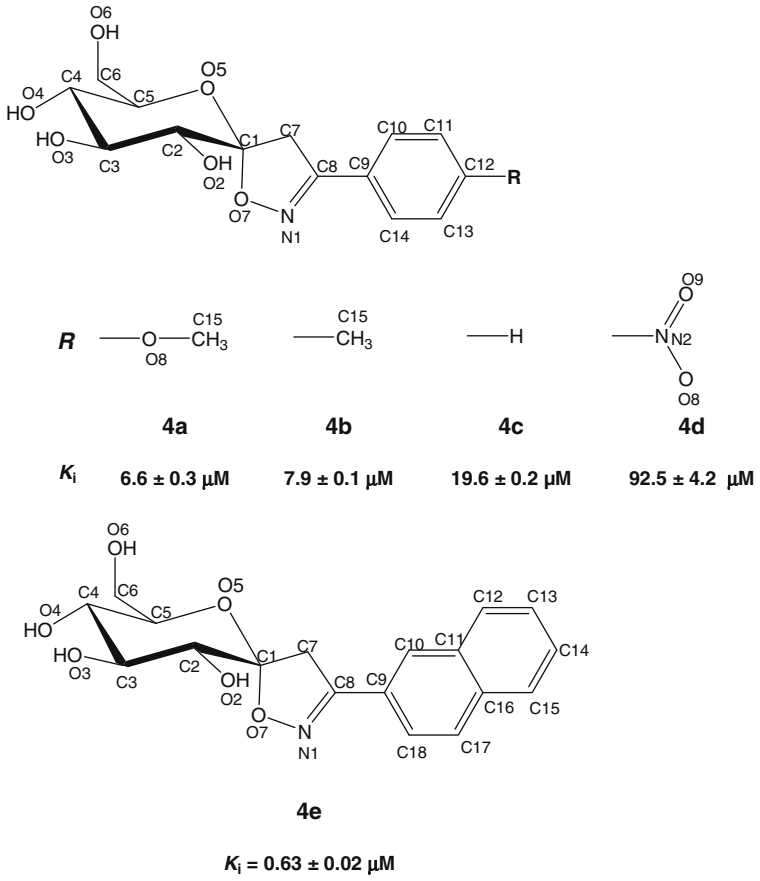

Figure 3. Chemical structures of glucopyranosylidene-spiro-isoxazoline **4a–e** compounds showing the numbering system used for X-ray crystallographic studies and the kinetic parameters (K_i values) for inhibition of GPb.

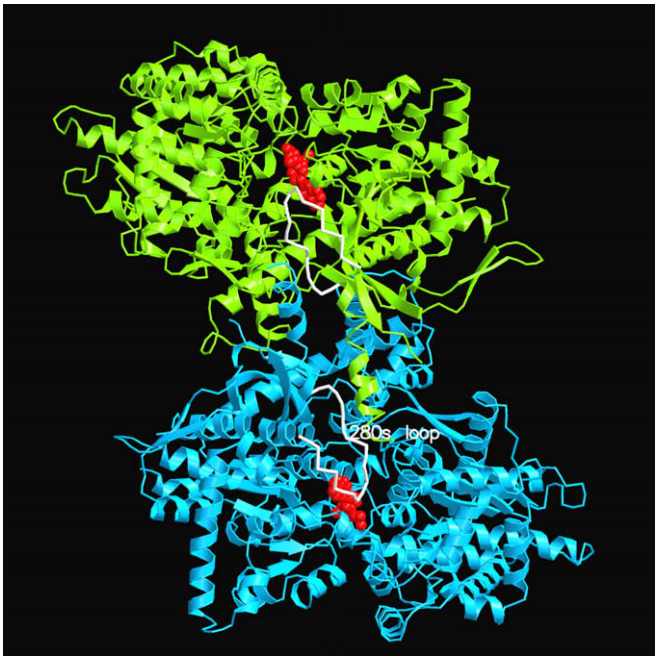

Figure 4. A schematic diagram of the GPb dimeric molecule, viewed down the molecular dyad. One subunit is colored in green and the other in blue. The position is shown for the catalytic site. The catalytic site, marked by (1*R*)-3′-(2-naphthyl)-spiro[1,5-anhydro-D-glucitol-1,5′-isoxazoline] (**4e**) (shown in red), is buried at the center of the subunit and is accessible to the bulk solvent through a 15 Å long channel. The inhibitor **4e** upon binding to the enzyme, promotes the less active T-state through stabilisation of the closed position of the 280s loop (shown in white).

the exception of **4b**, by inducing minor movements of the side chains of residues 282–287, of the 280s loop. The structural results also suggest a distortion of the five-membered ring where C1 is ~15° from the 4-atoms (O7–N1–C8–C7) plane. Below, we describe briefly the GPb/**4a–e** interactions (shown in Fig. 6) at the catalytic site. We start with compound **4c**, which carries the simplest group (-H) at the 4-position of the phenyl-spiro-isoxazoline moiety.

2.3.1. Compound 4c

There are no direct hydrogen bonding interactions between the atoms of the substituent introduced at C1 and the protein (Fig. 6c). O7 is hydrogen bonded to Asp283 OD2, Tyr573 OH, and Lys574 NZ through Wat214, and also to Gly135 N and Asp283 OD1 through another water molecule (Wat60). Also nitrogen atom N1 forms water-mediated interactions with Asn283 OD1 (through Wat290), and also with Glu88 OD2, Gly134 N, Gly137 N (through Wat80) (Table S10). The phenyl-spiro-isoxazoline analogue, on binding to GPb, makes a total of 14 hydrogen bonds and 79 van der Waals interactions, of which 11 are nonpolar/nonpolar contacts to Gly135, Leu136, and His341. In the T-state the catalytic site is partially blocked by the 280s loop, comprising residues 282–287 and in the GPb–**4c** complex the 280s loop retains its closed position by inducing only minor shifts of the side chains of Asn282, Asp283, and Asp284. Compound **4c** (K_i = 19.6 ± 0.2 μM) binds almost 87 times more tightly than α-D-glucose (K_i = 1.7 ± 0.1 mM),[11] possibly because of the additional interactions of the spiro-isoxazoline group with the protein.

2.3.2. Compound 4b

Introduction of a nonpolar methyl group in the 4-position of the phenyl-spiro-isoxazoline in compound **4b** increased the affinity for

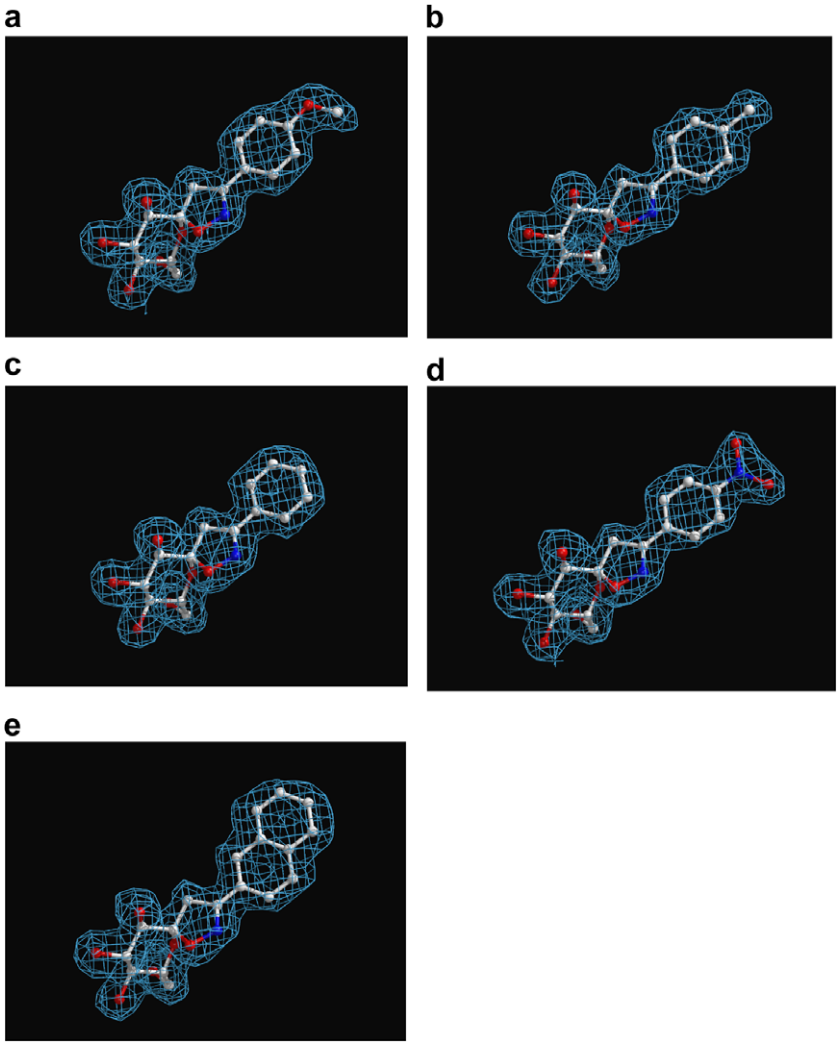

Figure 5. $2F_o - F_c$ electron density maps of **4a** (a), **4b** (b), **4c** (c), **4d** (d) and **4e** (e) structures bound at the catalytic site of GPb (from measurements at 293 K or, for **4b** and **4e** at 100 K). The maps are contoured at 1.0σ level. Electron density maps were calculated by using REFMAC[42] before incorporating ligand coordinates.

GPb by 2.5-fold (K_i = 7.9 ± 0.1 μM) compared to **4c**. Similar to GPb–**4c** binding, O7 and nitrogen N1 atoms make water-mediated interactions with Tyr573, Lys574, and Gly135 (through Wat458), and with Asp283, Glu88, Gly134, Ile136, and Gly137 (through Wat895) (Fig. 6b). **4b**, on binding to the enzyme, makes a total of 14 hydrogen bonds and 91 van der Waals interactions, 14 of which are nonpolar/nonpolar contacts to Gly135, Leu136, His341, and Asp283, which undergoes a conformational change. There is a shift in the 280s loop; the major shifts (compared to the GPb-α-D-glucose complex) for Cα atoms are for residues Asn282 (1.1 Å), Asp283 (1.4 Å), Asn284 (1.4 Å), Phe285 (2.1 Å), Phe286 (1.2 Å), and Glu287 (0.7 Å), and these shifts lead to increased contacts between Asp283 and **4b** phenyl ring atoms C10-C14 (Table S8). The 4-methyl group (C15) makes additional van der Waals contacts with His341 CE1 and NE2 (distance = 3.5 Å) and four water molecules (Wat282, Wat417, Wat896, Wat897).

It appears that upon binding of **4b** at the catalytic site, the 280s loop shifts to accommodate the 4-phenyl-spiro-isoxazoline moiety. Similar shifts of the 280s were observed previously on binding of *N*-benzoyl-*N*′-β-D-glucopyranosyl urea[43] and β-D-glucopyranosyl bismethoxyphosphoramidate[44] to the catalytic site of GPb in order to avoid steric clashes with Asn284.

The crystallographic binding experiment with **4b** was performed by soaking a single crystal of GPb with 30 mM **4b** in 10 mM Bes, pH 6.7, 30% (v/v) DMSO for 3.5 h (Table S2), prior to flash-cooling in the nitrogen steam (100 K). DMSO, which in solution promotes the R-state structure, was tested previously as a cryoprotectant in an experiment where native T-state GPb crystals were allowed to equilibrate for ~30 min with a buffered solution (pH 6.7) containing 10 mM Bes and 30% (v/v) DMSO, and a complete data set was collected at a maximum resolution of 2.3 Å.[45] The $F_o - F_c$ and $2F_o - F_c$ electron density maps indicated no binding of DMSO at the catalytic or at other regulatory binding sites, although in the 100 K DMSO GPb structure, the main-chain *B*-factor values for residues 283–285 were increased, compared to the room temperature T-state GP structure, from 26.7 to 48.1 Å^2.[45] In the present cryogenic experiment with **4b** (1.80 Å resolution) and **4e** (1.86 Å resolution), 16 and 15 molecules of DMSO were identified with average *B*-factor values of 40.4 and 43.0 Å^2, respectively, but none of these molecules bound at the catalytic site of the enzyme. On the contrary, cryogenic experiments with GPb using glycerol as a cryoprotectant[45–47] and GPa[48] have shown that glycerol binds at the catalytic site and competes with glucose analogues, thus preventing the formation of complexes. In the present work, a parallel investigation has been carried out with a single GPb crystal soaked for 2 h in a buffered solution (pH 6.7) containing 10 mM Bes and 30% (v/v) DMSO and data collected to 1.93 Å resolution.[49] The structural results showed that the residue Asn284 was not sup-

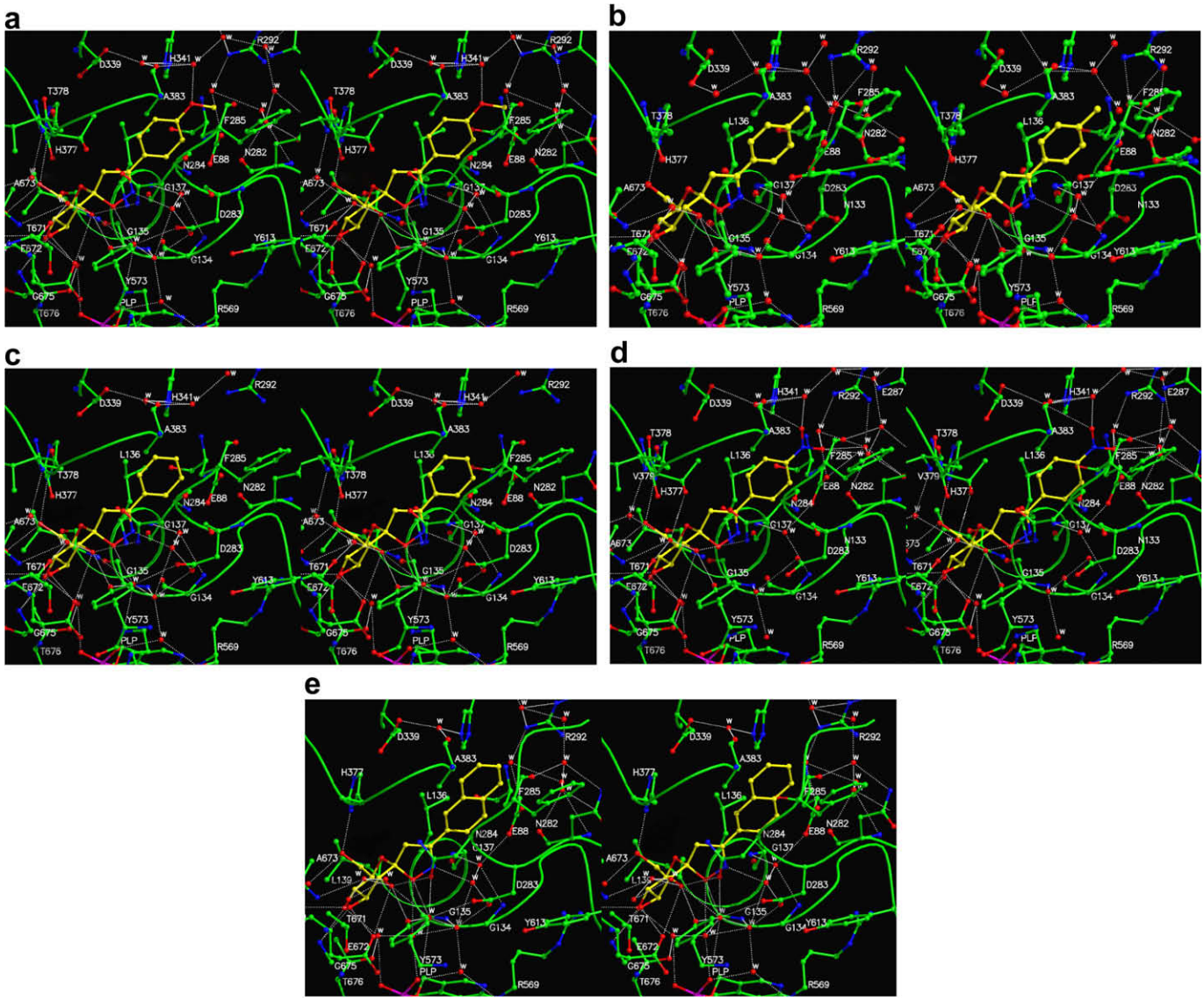

Figure 6. Stereo diagrams showing interactions between **4a** (a), **4b** (b), **4c** (c), **4d** (d) and **4e** (e) and protein in the vicinity of the catalytic site (from measurements at 293 K or, for **4b** and **4e** at 100 K). The hydrogen bonding pattern between ligands, protein residues and water molecules (w) in the catalytic site is represented by dotted lines.

ported in the electron density map, and little density was present to suggest a new position. Therefore, a clear conclusion cannot be drawn from the experimental and computational results (vide infra) whether the significant shifts in residues 282–287 observed in the GPb–**4b** structure arise from steric clashes of protein residues with **4b** or are correlated with the presence of 30% DMSO in the cryogenic crystallographic experiment. Most evidence does point to the latter but a combination of both factors is also possible.

2.3.3. Compound 4a

To improve the biological activity of **4b** we replaced the $-CH_3$ in the 4-position of the phenyl-spiro-isoxazoline with a methoxy substituent ($-OCH_3$), compound **4a**, based on the expectation that the addition of a polar group would induce additional hydrogen bonding interactions between the methoxy O8 and His341 NE2 and the water molecules in the vicinity of β-pocket. The new analogue was a slightly better inhibitor than **4b**, with a K_i value of 6.6 ± 0.3 μM, a result not as good as we expected. The structure of compound **4a** in complex with GPb was determined at 1.85 Å resolution, which revealed the detailed interactions of the ligand within the catalytic site. The water-mediated hydrogen bonding interactions of O7

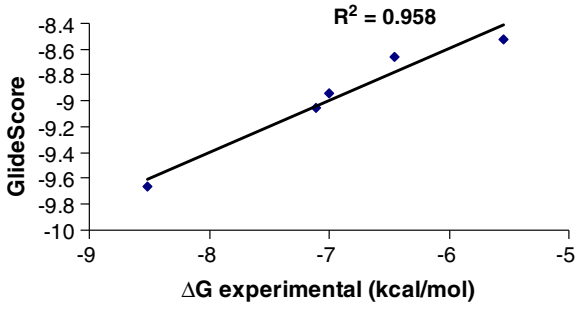

Figure 7. Correlation between GlideScores (GSs) and the experimental binding free energies obtained using the QPLD-XP docking algorithm with glucopyranose positional constraints and ESP fit ligand charges (in 'field' of receptor) for the **4a**–**e** ligands studied.

and N1 with Asp283, Tyr573, Lys574, Gly135, Glu88, Gly134, and Gly137 are maintained (Tables S3 and S4, Fig. 6a). In addition to these interactions, the methoxy O8 group forms a hydrogen bond with Ala383 O through Wat289, and also participates in a complex

hydrogen bonding network (through Wat222 and Wat102) (Table S4). The crystal structure of GPb–**4a** shows that O8 is not hydrogen bonded to His341 NE2, although O8 is at a hydrogen bonding distance from His341 NE2 (3.3 Å). The program CONTACT (CCP4) does not list this interaction due to a slight deviation of the allowed angle value for this bond (111°). As in the case of **4b**, the $-CH_3$ group (C15) makes van der Waals contacts with Asn282 O, Phe285 O, His341 CE1 and four water molecules (Wat194, Wat204, Wat274, Wat289), and it seems that this is not a favorable environment for a methyl group. The GPb–**4a** superimposes exactly with GPb–**4c** with respect to the position of the phenyl group, except that Wat276 (in GPb–**4c** structure) shifts by ~1.4 Å (Wat274 in GPb–**4a** structure) to avoid clashes with the $-CH_3$ group. Although the network of interactions is enhanced when the methoxy group is present, the affinity is only slightly improved (as compared with **4b**). Docking results replicate this finding and reveal a decreased Lipo-EvdW descriptor contribution to the docking GlideScore (vide infra: **Docking Results** and Fig. 8) within the β-cavity for a *para*-substituted phenyl with –OMe compared to –Me in **4b**.

2.3.4. Compound 4d

Introduction of a nitro group in the 4-position of the phenyl-spiro-isoxazoline, compound **4d**, showed that the affinity of this analogue for GPb, compared to that of the lead compound (**4c**), was significantly reduced (K_i = 92.5 ± 4.2 μM), although one would expect that the addition of a polar group would have the opposite effect. Oxygen atoms O8 and O9 of the 4-nitro group make water-mediated hydrogen bonding interactions with residues Glu88, Arg292, Tyr280, Asn282, Asp339, His341, and Ala383 (Table S12 and S13, Fig. 6d). Structural comparison between GPb–**4d** and GPb–**4c** complex structures showed that the atomic positions of C9–C14 of the phenyl group in the GPb–**4d** structure are shifted ~0.3–0.6 Å towards Asn282 O and Glu88 OE1. The new position of the 4-nitrophenyl group creates more space for the ligand to be accommodated at the β-pocket, causing displacement of two water molecules (Wat214 and Wat290 in GPb–**4c** structure) to avoid close contacts with C14, and also shifts of another two water molecules; Wat294 (in GPb–**4c** structure) shifted ~0.7 Å (Wat272 in GPb–**4d** structure) and Wat276 (in GPb–**4c** structure) shifted ~1.2 Å (Wat260 in GPb–**4d** structure). The 4-nitro-spiro-isoxazoline analogue **4d** on binding at the catalytic binding site of GPb makes a total of 16 hydrogen bonds and exploits 90 van der Waals interactions (10 nonpolar/nonpolar, 25 polar/polar, and 55 nonpolar/polar). Compound **4d** appears to form an improved network of interactions, however it exhibits poorer affinity than the lead molecule (**4c**); this may be due to the changes observed in the water structure and again as in the case of **4a**, that a polar *para*-phenyl substituent is non-optimal with regard to non-bond interactions as defined by the docking Lipo-EvdW contribution (vide infra: **Docking Results** and Fig. 8). There were also indications in both $2F_o - F_c$ and $F_o - F_c$ electron density difference maps for weak binding of compound **4d** at the inhibitor site, which is formed by two hydrophobic aromatic residues, Phe285 and Tyr613, and is located at the surface of the protein molecule; the site has been shown to bind purines, nucleosides, nucleotides, and heterocyclic compounds.[6,7,45] The electron density at the inhibitor site was not well resolved to indicate the binding mode of the ligand. In a crystallographic experiment with 2 mM **4d** (17 h soaking of GPb crystals in 10 mM Bes, 2% DMSO buffer, pH 6.7) (data not shown), electron density maps indicated strong binding of **4d** at the catalytic site, but very poor electron density at the inhibitor site. It seems therefore, that the catalytic site is indeed the primary binding site for **4d**.

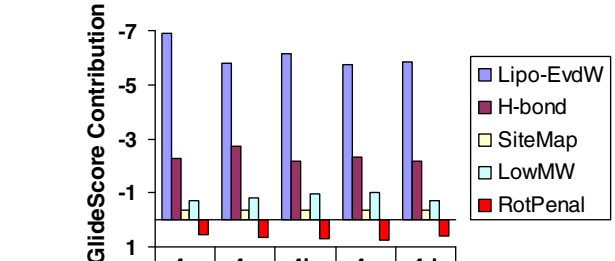

	4e	4a	4b	4c	4d
Lipo-EvdW	-6.92	-5.77	-6.15	-5.72	-5.84
H-bond	-2.26	-2.72	-2.19	-2.34	-2.17
SiteMap	-0.35	-0.36	-0.36	-0.36	-0.36
LowMW	-0.7	-0.83	-0.94	-1	-0.73
RotPenal	0.57	0.63	0.69	0.75	0.58

Figure 8. Breakdown of the individual XP term contributions to the GlideScores (GSs) for binding of each ligand obtained using QPLD-XP docking with glucopyranose positional constraints and with ESP fit charges calculated in the 'field' of the receptor. The best GS is the most negative, hence large negative contributions are the most favorable. The highest to lowest scoring ligands are displayed in order from left (**4e**) to right (**4d**).

2.3.5. Compound 4e

Compound **4e**, the most active spiro-isoxazoline derivative, revealed a 2700-fold improvement in enzymic activity, when compared to α-D-glucose (K_i = 1.7 ± 0.1 mM) and is one of the most potent known inhibitors of muscle GPb[6,7] that binds at the catalytic site. The structure of compound **4e** was determined at 1.86 Å resolution, in the presence of 30% DMSO, under cryogenic conditions (100 K). In contrast to **4b**, the structural results with **4e** show that the ligand interacts directly with main-chain or/and sidechain of Asn282, Asn284, Phe285, and indirectly with the carboxylates OD1 and OD2 of Asp283, holding the 280s loop in its closed T-state conformation and therefore competing with any possible effects of the allosteric effector DMSO on the TR allosteric equilibrium. The water-mediated hydrogen bonding interactions of O7 with Asp283, Tyr573, Lys574, and Gly135, and those of N1 with Glu88, Gly134, and Gly137 are also maintained in the GPb–**4e** complex structure (Tables S15 and S16) (Fig. 6e). Overall, **4e** makes a total of 15 hydrogen bonds and 111 van der Waals interactions (17 nonpolar/nonpolar, 15 polar/polar, 79 polar/nonpolar) (Table S17), of which 40 are contacts to the 2-naphthyl group. Superposition of the **4c** and **4e** compounds bound at the catalytic site shows that the 2-naphthyl group of **4e** is inclined ~11° with respect to the phenyl group of **4c** in order to minimize close contacts with His341; also some rearrangement of the water structure in the vicinity of the β-pocket involved Wat294 (in the GPb–**4c** structure) which was displaced, and water molecules Wat276 (Wat409 in the GPb–**4e** structure), Wat226 (Wat404 in the GPb–**4e** structure) and Wat198 (Wat333 in the GPb–**4e** structure) which shifted ~1.2, 0.5, and 1.1 Å, respectively, to optimize contacts with the 2-naphthyl group. The inhibition constant of **4e** for rabbit muscle GPb is K_i = 0.63 ± 0.02 μM, ~30 times decreased than the lead compound **4c**, indicating a difference in the binding free energy between **4e** and **4c** of about 2.1 kcal/mol. A major contribution to the difference in the binding affinity between **4e** and lead compound **4c** may result from the extended interactions of the 2-naphthyl group with protein atoms and the water hydrogen-bonding network in the vicinity of the β-pocket. The output from docking calculations is more revealing in this aspect.

2.4. Docking results

The GPb enzyme was prepared for docking using the coordinates of GPb:**4e** co-crystallized complex with Schrödingers 'Protein

Table 1
Comparison of docking performance using default OPLS-AA(2001) forcefield ligand charges (GLIDE-XP) or electrostatic potential (ESP) fit ligand charges (QPLD-XP) and different docking constraints with respect to reproduction of the crystallographic ligand binding conformations[a]

Ligand	GLIDE-XP OPLS-AA(2001) charges			QPLD-XP ESP fit charges (gas phase)	QPLD-XP ESP fit charges (field receptor)
Constraints	None	Core	(i) Core (ii) O(H)	(i) Core (ii) O(H)	(i) Core (ii) O(H)
4a	0.655	0.655	0.654	0.656	0.555
4b	1.210	0.476	0.477	0.477	0.473
4c	0.435	0.430	0.436	0.554	0.434
4d	0.506	0.499	0.498	0.671	0.499
4e	1.502	1.498	1.498	1.503	1.498
Average	0.862	0.712	0.713	0.772	0.692

[a] Measured as root-mean-square-distance (RMSD) in Å between superimposed heavy atoms from the top-ranked binding poses and the crystallographic ligand conformations. Docking positional constraints were on the glucopyranose moiety: (i) core constraints (1 Å) on the glucopyranose ring atoms; (ii) positional constraints (radius 1 Å) on the O(H) oxygen atoms based on their positions in the **4e** complex.

Preparation Wizard' as described in Section 4.5. In our previous benchmark study,[19] we found that the inclusion of cavity waters, albeit crucial in flexible receptor–ligand molecular dynamics (MD) calculations, was not important in rigid receptor docking calculations. Based on these results, no crystallographic waters were retained in the current study. Different docking algorithms were probed for their effectiveness in reproducing crystallographic and kinetic data. Results for the superimposition of the top-ranked ligand binding poses on the crystallographic conformations for these docking algorithms (GLIDE-XP and QPLD-XP) using different glucopyranose positional constraints and ligand partial charges are shown in Table 1, while the correlation between the docking GSs and experimental binding free energies are shown in Table 2.

For the GLIDE-XP docking runs using OPLS-AA(2001) partial charges and no docking constraints, it appears that excellent correlation (R^2 = 0.878) for the docking GSs—experimental binding free energies has been attained. However, superimposing the top-ranked ligand docking poses for ligands **4a–e** and their crystallographic binding conformations, we see that the results for two of the ligands (**4b** and **4e**) are not within the desired accuracy threshold with RMSDs (heavy atoms) >1.0 Å. In the case of **4b** the crystallographic conformation was ranked as the second best pose with a corresponding docking score (GS) = −9.04. This could be attributed to the rigid-docking protocol, which ignores the protein conformational changes and shift in 280's loop occurring upon binding of **4b**. The top-ranked pose had an almost identical score (GS = −9.05) with the crystallographic conformation but was significantly different to the crystallographic conformations (RMSD (heavy atoms) = 1.210 Å (Table 1)). This is in contrast to a clear-cut distinction between the GSs for correct and incorrect binding poses compared to crystallography for all other ligands. On imposing glucopyranose positional constraints in the docking calculations, the crystallographic ligand binding conformation was now ranked first and excellent correlation for docking GS versus experimental binding free energy for all ligands (including **4b**) obtained, indicating that the receptor conformation from the **4e** complex is also consistent with favorable **4b** binding. For **4e**, although the RMSD is 1.506 Å, the larger RMSD is due to a flip in an otherwise close to superimposable naphthyl moiety. Nevertheless, the incorrect top-ranked binding pose for **4b** (RMSD = 1.210 Å) shows that an excellent correlation with relative binding affinities does not always constitute a proof of successful binding prediction. Application of docking positional constraints on the glucopyranose moiety ensured that the ligands adopted their correct and well-defined positions in the catalytic site and gave rise to better predicted ligand binding conformations. Its application also ensured greater computational efficiency in searching for correct binding poses and not unrealistic glucopyranose positions/orientations. Two types of positional constraints were used: **core** constraints on the glucopyranose 6-membered ring positions with a tolerance of 1 Å from their reference positions which was the **4e** ligand in the prepared **4e** complex; and positional constraints (denoted **O(H)** in Tables 1 and 2) on the glucopyranose oxygen atoms which were restricted to spheres with radius 1 Å around their reference positions. Once these constraints were applied, more accurate ligand binding conformations were obtained using both GLIDE-XP with OPLS-AA(2001) charges and QPLD-XP where the GLIDE-XP poses were redocked using ESP fit charges. There was not a significant difference in performance of the algorithms GLIDE-XP and QPLD-XP using docking constraints with respect to reproduction of the ligand crystallographic conformations with average RMSDs ranging between 0.692 and 0.772 Å. QPLD-XP using ESP fit charges in the 'field' of the receptor performed best (RMSD = 0.692 Å) in this regard. Inspection of the top-ranking poses reveals the expected glucopyranose moiety hydrogen bonds are close to intact (elongated in a few cases) for all ligands. This was also the case in our previous GLIDE-XP docking calculations.[19] With respect to the correlation between top-ranked docking scores and experimental binding free energies, there is a more significant difference in performance between GLIDE-XP and QPLD-XP using constraints. While GLIDE-XP docking with OPLS-AA(2001) ligand charges produces good correlations (R^2 = 0.782; 0.722), the correlation obtained redocking the GLIDE-XP ligand poses with ESP fit charges calculated in the gas phase using QM (R^2 = 0.848) or in the 'field' of the receptor using QM/MM (R^2 = 0.958) is excellent (Fig. 7).

GLIDE uses a crude explicit water model for modeling solvation effects.[17,18] Our results show that this model is indeed very effective. However, caution here should be used, as the pseudo-explicit water molecules are placed after the initial docking and therefore

Table 2
Comparison of docking performance using the different algorithms, ligand charges and docking constraints with respect to correlation between the docking GlideScores (GSs) and experimental binding free energies for ligands **4a–e**

Docking algorithm	Ligand charges	Constraints[a]	Correlation coefficient (R^2)
GLIDE-XP	OPLS-AA(2001)	—	0.878
GLIDE-XP	OPLS-AA(2001)	Core	0.782
GLIDE-XP	OPLS-AA(2001)	Core + O(H)	0.722
QPLD-XP	ESP fit (gas phase)	Core + O(H)	0.848
QPLD-XP	ESP fit ('field' of receptor)	Core + O(H)	0.958

[a] Constraints on glucopyranose moiety—core constraints (1 Å) on the glucopyranose ring atoms; positional constraints (radius 1 Å) on the O(H) oxygen atoms based on their positions in the **4e** complex.

may not be the best tool for predicting conserved water molecules. In terms of overall performance, the QPLD-XP method with constraints on the glucopyranose moiety was best in terms of correct binding conformations and GS—experimental binding free energy correlation. At least for this small ligand set tested, the ESP fit charges calculated in the field of the receptor, yielded superior results to the free ligand gas phase ESP fit charges which also gave very good results. Additional tests with larger ligands sets, however, are necessary to confirm the transferability of this assertion. Nevertheless, standard GLIDE-XP with OPLS-AA(2001) charges and docking constraints on the glucopyranose moiety appears a fast-track method for screening larger databases of ligands, the top poses which then can be redocked more accurately using QPLD-XP. It should also be noted that as docking is limited by conformational sampling, it is important for greater accuracy to use a number of different ligand input conformations.

2.4.1. Breakdown of individual GlideScore (GS) descriptor contributions to ligand binding affinities

Given the accuracy of the docking results obtained, we decided to decipher the descriptor components of GSs for each ligand into their individual contributions using XP-Visualizer, to obtain useful information or clues for the design of more potent inhibitors. For this purpose, the GSs of most successful docking algorithm and method were used: QPLD-XP with ESP fit ligand charges calculated in the 'field' of the receptor and employing docking constraints on the glucopyranose moiety positions. Correlation of $R^2 = 0.958$ between docking scores and experimental binding free energies was obtained (Fig. 7). The break down of descriptor information is depicted graphically and in tabular form in Figure 8.

GlideScore is an empirical scoring function[17] based on ChemScore,[50] but modified and extended. The XP descriptors of relevance used to score our set of ligands were *Lipo-EvdW*, *H-bond*, *SiteMap*, *LowMW*, and *RotPenal*. The *Lipo-EvdW* descriptor is the ChemScore lipophilic pair term and fraction of the total receptor-ligand van der Waals energy; H-bond is the ChemScore H-bonding pair term; *SiteMap* scores the ligand/receptor non-H-bonding polar/hydrophobic interactions following generation of hydrophobic–hydrophilic surfaces; *LowMW* rewards for ligands with low molecular weight (MW); and *RotPenal* penalizes for ligand rotable bonds.[51]

Lipo-EvdW is the major contributor to the final GSs, as clearly indicated in Figure 8. The term is highest for the ligands **4e** (−6.92) and **4b** (−6.15) with nonpolar substituents in the β-cavity, naphthyl and *p*-Me-phenyl, respectively. *para*-Substitution of the phenyl groups with polar substituents is not favorable with much lower *Lipo-EvdW* contributions for **4a** (−5.77) and **4d** (−5.84), and close to that for an unsubstituted phenyl moiety (**4c** (−5.72)). The H-bond contribution for **4a** with the *para*–OMe phenyl susbtituent is highest (−2.72) forming a H-bond with Phe285 and close to a direct H-bond with His341, but **4d** with a $-NO_2$ *para*-phenyl substituent is poorest (−2.17) and forms only water-mediated H-bonds as seen in the crystal structure (vide supra). The *SiteMap* term is approximately identical across the set of ligands. For the *LowMW* term, although ligand **4e** is penalized with respect to the other ligands for its bulkier/heavier naphthyl substituent, the gains elsewhere are clear to be seen. Finally, for the *RotPenal* term, the penalty contribution for restricting rotation of the (*para*-substituted) phenyl and naphthyl moieties is lowest (∼+0.57) for **4e** (naphthyl rotation) and the *p*-NO_2 phenyl moiety in **4d**, and highest for the more flexible unsubstituted phenyl moiety (+0.75) of **4b**. Overall, the ligand **4e** binds strongest due to its nonpolar and rigid aromatic ring moiety. On this basis, substituted naphthyl groups or more extended rigid aromatic groups should be investigated as putative more potent inhibitors. Work in this area is currently under way.

3. Conclusion

In conclusion, a new series of spiro-isoxazoline compounds were designed, synthesized and tested for inhibition and crystallographic binding to GPb. All the inhibitors bound at the catalytic site of the enzyme, promoting the less active T-state conformation through an extended network of hydrogen bond interactions with protein residues in the vicinity of the same site. They all induced only minor shifts upon binding except **4b** that causes more profound changes to avoid steric clashes with Asn284. Compound **4e** was found to be the most potent inhibitor among the five compounds with a K_i value of 0.63 M that may be attributed to both the rigidity of the spiro and 2-naphthyl groups that undergo little loss of conformational entropy on binding and to the extended network of interactions formed. The rigid receptor docking calculations with glucopyranose positional constraints accurately reproduced ligand crystallographic binding conformations and produced excellent correlation between top-ranked ligand docking score and experimental binding free energies. Although good results were obtained with OPLS-AA(2001) ligand partial charges, there was a significant improvement using ESP fit ligand charges in the QPLD-XP calculations. For the latter, ESP fit charges in the 'field' of the receptor yielded superior results compared to those calculated for the free ligand in the gas phase. Our ligand data set was admittedly small and, therefore, the success levels of the methods must be treated with some scepticism as regards to their application to larger ligand data sets and standalone predictability of ligand binding affinities. Nevertheless, the small data set here allowed us to analyze results in more detail and served as another benchmark for developing an optimum protocol for docking at the catalytic site of GP, carrying on from our previous work.[19] A trade off between accuracy versus computational expense must be considered in the choice between GLIDE-XP using default OPLS-AA (2001) atomic partial charges or the more computationally expensive QPLD-XP method for future applications. However, the methods employed here can investigate the docking conformations and relative binding affinities of a series of GP complexes with good accuracy and significantly less computational effort, compared to full-scale molecular dynamics free-energy simulations.[52]

4. Experimental section

4.1. General methods

Thin-layer chromatography (TLC) was carried out on aluminum sheets coated with Silica Gel 60 F_{254} (Merck). TLC plates were inspected by UV light ($\lambda = 312$ nm) and developed by treatment with a mixture of 10% H_2SO_4 in EtOH/H_2O (1:1 v/v) followed by heating. Silica gel column chromatography was performed with Geduran® Silica Gel Si 60 (40–63 μm) purchased from Merck (Darmstadt, Germany). Preparative reversed phase chromatography (RP-18) was performed using a 15 × 150 mm column of fully endcapped Silica Gel 100 C_{18} (>400 mesh, Fluka). ^1H and ^{13}C NMR spectra were recorded at 23 °C using Bruker Advance DRX300 or DRX500 spectrometers with the residual solvent as the internal standard. The following abbreviations are used to explain the observed multiplicities: s, singlet; d, doublet; dd, doublet of doublet; ddd, doublet of doublet of doublet; t, triplet; td, triplet of doublet; q, quadruplet; m, multiplet; br, broad; p, pseudo. Structure elucidation was deduced from 1D and 2D NMR spectroscopy which allowed, in most cases, complete signal assignments based on COSY, HSQC, and HMBC correlations. NMR solvents were purchased from Eurisotop (Saint Aubin, France). HRMS (LSIMS) mass spectra were recorded in the positive mode using a Thermo Finnigan Mat 95 XL spectrometer. MS (ESI) mass spectra were recorded in the positive

mode using a Thermo Finnigan LCQ spectrometer. Optical rotations were measured using a Perkin–Elmer polarimeter.

4.1.1. [3+2]-Cycloaddition of aromatic nitrile oxides to *exo*-glucals (Method A)

A solution of *exo*-glucal **2** (0.3 mmol) and α-chloroarylaldoxime (1.5 mmol, 5 equiv) in CH_2Cl_2 (5 mL) was stirred at rt under Argon. Triethylamine (2.25 mmol, 7.5 equiv) was dissolved in CH_2Cl_2 (5 mL) and slowly added dropwise in 5 h with a syringe pump. The reaction was stirred at rt for an additional 12 h then the solvent was evaporated. The residue was purified by flash silica gel column chromatography to afford the desired cycloadducts **3a**–**e**.

4.1.2. Zemplén deacetylation (Method B)

A solution of the acetyl-protected carbohydrate derivatives **3a**–**e** (0.15 mmol) and NaOMe (50 μL, 1 M in MeOH) in MeOH (3 mL) was stirred at rt for 3 h. The solution was then neutralized to pH 5 with a cation exchange resin (DOWEX 50WX2, H^+ form). The resin was filtered off and washed with MeOH (3 × 10 mL) then the filtrate was evaporated off. The residue was purified by flash silica gel column chromatography to afford the desired hydroxylated carbohydrate derivatives **4a**–**e**.

4.2. Syntheses of glucose-based inhibitors

4.2.1. 3,4,5,7-Tetra-*O*-acetyl-2,6-anhydro-1-deoxy-D-gluco-hept-1-enitol (2)[39]

A solution of 3,4,5,7-tetra-*O*-triethylsilyl-2,6-anhydro-1-deoxy-D-gluco-hept-1-enitol[37] (526 mg, 0.83 mmol) in tetrabutylammonium fluoride (4.16 mL, 1 M in THF) was stirred at room temperature for 4 h. The solution was then diluted with pyridine (4 mL) and acetic anhydride (2 mL). The reaction mixture was stirred at rt for 16 h. The solution was poured into iced water (100 mL) and the aqueous layer extracted with EtOAc (3 × 150 mL). The organic layers were combined, dried ($MgSO_4$) and evaporated. The residue was purified by flash silica gel column chromatography (PE/EtOAc, 7:3) to afford **2**[39] (250 mg, 87%) as a colorless syrup.

4.2.2. (5*R*,7*R*,8*R*,9*S*,10*R*)-8,9,10-Tris(acetoxy)-7-[(acetoxy)methyl]-3-(4-methoxyphenyl)-1,6-dioxa-2-azaspiro[4,5]dec-2-ene (3a)

A solution composed of **2** (55 mg, 0.16 mmol), α-chloro-4-methoxybenzaldoxime (89 mg, 0.48 mmol) and triethylamine (100 μL, 0.72 mmol) was treated according to method A. The residue was purified by flash silica gel column chromatography (PE/EtOAc, 3:2) to afford **3a** (65 mg, 83%) as a white solid. R_f = 0.23 (PE/EtOAc, 3:2); mp = 68–69 °C (CH_2Cl_2/EP); $[\alpha]_D^{20}$ = +75 (*c* 1, $CHCl_3$); ^{1}H NMR (300 MHz, $CDCl_3$) δ 2.00 (s, 3H, CH_3), 2.04 (s, 3H, CH_3), 2.05 (s, 3H, CH_3), 2.06 (s, 3H, CH_3), 3.29 (d, 1H, *J* = 17.7 Hz, H-4a), 3.38 (d, 1H, *J* = 17.7 Hz, H-4b), 3.83 (s, 3H, OCH_3), 4.03 (dd, 1H, *J* = 2.0 Hz, *J* = 12.6 Hz, C*H*$_2$OAc), 4.27 (dd, 1H, *J* = 3.7 Hz, *J* = 12.6 Hz, C*H*$_2$OAc), 4.34 (ddd, 1H, *J* = 2.0 Hz, *J* = 3.7, *J* = 10.1 Hz, H-7), 5.19 (dd, 1H, *J* = 9.5 Hz, *J* = 10.1 Hz, H-8), 5.41 (d, 1H, *J* = 10.0 Hz, H-10), 5.53 (dd, 1H, *J* = 10.0 Hz, *J* = 9.5 Hz, H-9), 6.91 (d, 2H, *J* = 8.9 Hz, H-ar), 7.58 (d, 2H, *J* = 8.9 Hz, H-ar); ^{13}C NMR (75 MHz, $CDCl_3$) δ 20.58 (CH_3), 20.59 (CH_3), 20.6 (CH_3), 20.7 (CH_3), 43.5 (C-4), 55.4 (OCH_3), 61.4 (*C*H$_2$OAc), 67.8 (C-8), 69.1 (C-10), 69.2 (C-7), 71.6 (C-9), 106.7 (C-5), 114.2 (s, 2C, CH-ar), 120.6 (C-ar), 128.5 (s, 2C, CH-ar), 157.3 (C-3), 161.6 (C-ar), 169.6, 169.8, 170.3, 170.6 (4s, O*C*OCH$_3$); MS (ESI) *m*/*z* = 493.9 $[M+H]^+$, 516.0 $[M+Na]^+$, 986.6 $[2M+H]^+$, 1008.7 $[2M+Na]^+$; HRMS (ESI) *m*/*z* = $C_{23}H_{27}NO_{11}Na$ $[M+Na]^+$ calcd 516.1481, found 516.1488.

4.2.3. (5*R*,7*R*,8*R*,9*S*,10*R*)-8,9,10-Tris(acetoxy)-7-[(acetoxy)methyl]-3-(4-toluyl)-1,6-dioxa-2-azaspiro[4,5]dec-2-ene (3b)

A solution composed of **2** (105 mg, 0.30 mmol), α-chloro-4-methybenzaldoxime (260 mg, 1.52 mmol) and triethylamine (320 μL, 2.30 mmol) was treated according to method A. The residue was purified by flash silica gel column chromatography (PE/EtOAc, 7:3) to afford **3b** (138 mg, 95%) as a pale yellow foam. R_f = 0.22 (PE/EtOAc, 7:3); $[\alpha]_D^{20}$ = +57 (*c* 1, CH_2Cl_2); ^{1}H NMR (300 MHz, $CDCl_3$) δ 2.02 (s, 3H, CH_3), 2.05 (s, 3H, CH_3), 2.06 (s, 3H, CH_3), 2.07 (s, 3H, CH_3), 2.39 (s, 3H, PhC*H*$_3$), 3.31 (d, 1H, *J* = 17.8 Hz, H-4a), 3.41 (d, 1H, *J* = 17.8 Hz, H-4b), 4.05 (d, 1H, *J* = 10.8 Hz, C*H*$_2$OAc), 4.28 (m, 1H, C*H*$_2$OAc), 4.30 (m, 1H, H-7), 5.21 (dd, 1H, *J* = 9.6 Hz, *J* = 9.9 Hz, H-8), 5.42 (d, 1H, *J* = 10.1 Hz, H-10), 5.55 (dd, 1H, *J* = 10.1 Hz, *J* = 9.6 Hz, H-9), 7.22 (d, 2H, *J* = 8.1 Hz, H-ar), 7.54 (d, 2H, *J* = 8.1 Hz, H-ar); ^{13}C NMR (75 MHz, $CDCl_3$) δ 20.50 (CH_3), 20.53 (CH_3), 20.57 (CH_3), 20.64 (CH_3), 21.4 (Ph*C*H$_3$), 43.4 (C-4), 61.4 (*C*H$_2$OAc), 67.8 (C-8), 69.1 (C-10), 69.3 (C-7), 71.6 (C-9), 106.8 (C-5), 125.3 (C-ar), 126.7 (s, 2C, CH-ar), 129.5 (s, 2C, CH-ar), 141.3 (C-ar),157.6 (C-3), 169.5, 169.7, 170.2, 170.5 (4s, O*C*OCH$_3$); MS (ESI) *m*/*z* = 477.8 $[M+H]^+$, 500.0 $[M+Na]^+$, 954.6 $[2M+H]^+$, 976.6 $[2M+Na]^+$; HRMS (ESI) *m*/*z* = $C_{23}H_{28}NO_{10}$ $[M+H]^+$ calcd 478.1713, found 478.1718.

4.2.4. (5*R*,7*R*,8*R*,9*S*,10*R*)-8,9,10-Tris(acetoxy)-7-[(acetoxy)methyl]-3-(phenyl)-1,6-dioxa-2-azaspiro[4,5]dec-2-ene (3c)

A solution composed of **2** (51 mg, 0.15 mmol), α-chlorobenzaldoxime (115 mg, 0.74 mmol) and triethylamine (155 μL, 1.10 mmol) was treated according to method A. The residue was purified by flash silica gel column chromatography (PE/EtOAc, 3:2) to afford **3c** (67 mg, 99%) as a white solid. R_f = 0.25 (PE/EtOAc, 3:2); mp = 55–56 °C (CH_2Cl_2/EP); $[\alpha]_D^{20}$ = +60 (*c* 1, $CHCl_3$); ^{1}H NMR (300 MHz, $CDCl_3$) δ 2.00 (s, 3H, CH_3), 2.03 (s, 3H, CH_3), 2.04 (s, 3H, CH_3), 2.06 (s, 3H, CH_3), 3.31 (d, 1H, *J* = 17.8 Hz, H-4a), 3.41 (d, 1H, *J* = 17.8 Hz, H-4b), 4.02 (d, 1H, *J* = 11.1 Hz, C*H*$_2$OAc), 4.27 (m, 1H, C*H*$_2$OAc), 4.34 (m, 1H, H-7), 5.19 (t, 1H, *J* = 9.7 Hz, *J* = 9.7 Hz, H-8), 5.42 (d, 1H, *J* = 10.1 Hz, H-10), 5.54 (dd, 1H, *J* = 10.1 Hz, *J* = 9.7 Hz, H-9), 7.42 (m, 3H, H-ar), 7.63 (m, 2H, H-ar); ^{13}C NMR (75 MHz, $CDCl_3$) δ 20.53 (CH_3), 20.56 (CH_3), 20.6 (CH_3), 20.7 (CH_3), 43.3 (C-4), 61.4 (*C*H$_2$OAc), 67.7 (C-8), 69.1 (C-10), 69.4 (C-7), 71.5 (C-9), 106.9 (C-5), 126.8 (s, 2C, CH-ar), 128.2 (C-ar), 128.8 (s, 2C, CH-ar), 130.9 (C-ar), 157.7 (C-3), 169.5, 169.7, 170.2, 170.6 (4s, O*C*OCH$_3$); MS (ESI) *m*/*z* = 463.9 $[M+H]^+$, 486.0 $[M+Na]^+$, 948.7 $[2M+Na]^+$; HRMS (ESI) *m*/*z* = $C_{22}H_{25}NO_{10}Na$ $[M+Na]^+$ calcd 486.1376, found 486.1378.

4.2.5. (5*R*,7*R*,8*R*,9*S*,10*R*)-8,9,10-Tris(acetoxy)-7-[(acetoxy)methyl]-3-(4-nitrophenyl)-1,6-dioxa-2-azaspiro[4,5]dec-2-ene (3d)

A solution composed of **2** (43 mg, 0.12 mmol), α-chloro-4-nitrobenzaldoxime (124 mg, 0.62 mmol) and triethylamine (130 μL, 0.93 mmol) was treated according to method A. The residue was purified by flash silica gel column chromatography (PE/EtOAc, 3:2) to afford **3d** (59 mg, 94%) as a pale yellow solid. R_f = 0.25 (PE/EtOAc, 3:2); mp = 119–120 °C (CH_2Cl_2/EP); $[\alpha]_D^{20}$ = +58 (*c* 1, $CHCl_3$); ^{1}H NMR (300 MHz, $CDCl_3$) δ 2.00 (s, 3H, CH_3), 2.03 (s, 3H, CH_3), 2.04 (s, 3H, CH_3), 2.05 (s, 3H, CH_3), 3.33 (d, 1H, *J* = 17.9 Hz, H-4a), 3.44 (d, 1H, *J* = 17.9 Hz, H-4b), 4.05 (d, 1H, *J* = 10.8 Hz, C*H*$_2$OAc), 4.26 (m, 1H, C*H*$_2$OAc), 4.32 (m, 1H, H-7), 5.21 (dd, 1H, *J* = 9.4 Hz, *J* = 10.0 Hz, H-8), 5.43 (d, 1H, *J* = 10.1 Hz, H-10), 5.54 (dd, 1H, *J* = 10.1 Hz, *J* = 9.4 Hz, H-9), 7.81 (d, 2H, *J* = 8.9 Hz, H-ar), 8.26 (d, 2H, *J* = 8.9 Hz, H-ar); ^{13}C NMR (75 MHz, $CDCl_3$) δ 20.50 (CH_3), 20.52 (CH_3), 20.57 (CH_3), 20.64 (CH_3), 42.8 (C-4), 61.3 (*C*H$_2$OAc), 67.6 (C-8), 69.1 (C-10), 69.7 (C-7), 71.4 (C-9), 107.8 (C-5), 124.1 (s, 2C, CH-ar), 127.7 (s, 2C, CH-ar), 134.2 (C-ar), 148.9 (C-ar),156.2 (C-3), 169.5, 169.7, 170.1, 170.5 (4s, O*C*OCH$_3$); MS (ESI) *m*/*z* = 508.8 $[M+H]^+$, 531.0 $[M+Na]^+$, 1038.6 $[2M+Na]^+$; HRMS (ESI) *m*/*z* = $C_{22}H_{24}N_2O_{12}Na$ $[M+Na]^+$ calcd 531.1227, found 531.1224.

4.2.6. (5*R*,7*R*,8*R*,9*S*,10*R*)-8,9,10-Tris(acetoxy)-7-[(acetoxy)methyl]-3-(2-naphthyl)-1,6-dioxa-2-azaspiro[4,5]dec-2-ene (3e)

A solution composed of **2** (100 mg, 0.29 mmol), α-chloro-2-naphthaldoxime (296 mg, 1.40 mmol) and triethylamine (300 μL,

2.15 mmol) was treated according to method A. The residue was purified by flash silica gel column chromatography (PE/EtOAc, 3:1) to afford **3e** (140 mg, 94%) as a pale yellow foam. R_f = 0.28 (PE/EtOAc, 3:1); $[\alpha]_D^{20}$ = +39 (*c* 1, CH_2Cl_2); ^{1}H NMR (300 MHz, $CDCl_3$) δ 2.01 (s, 3H, CH_3), 2.04 (s, 3H, CH_3), 2.04 (s, 3H, CH_3), 2.05 (s, 3H, CH_3), 3.43 (d, 1H, *J* = 17.7 Hz, H-4a), 3.54 (d, 1H, *J* = 17.7 Hz, H-4b), 4.05 (m, 1H, CH_2OAc), 4.25 (m, 2H, H-7 CH_2OAc), 5.22 (t, 1H, *J* = 9.7 Hz, *J* = 9.7 Hz, H-8), 5.46 (d, 1H, *J* = 10.1 Hz, H-10), 5.57 (dd, 1H, *J* = 10.1 Hz, *J* = 9.7 Hz, H-9), 7.50 (m, 2H, H-ar), 7.90 (m, 5H, H-ar); ^{13}C NMR (75 MHz, $CDCl_3$): δ = 20.48 (CH_3), 20.51 (CH_3), 20.55 (CH_3), 20.62 (CH_3), 43.2 (C-4), 61.4 (CH_2OAc), 67.7 (C-8), 69.1 (C-10), 69.4 (C-7), 71.5 (C-9), 107.0 (C-5), 123.0 (CH-ar), 125.7 (C-ar), 127.5, 127.6, 127.8, 128.3, 128.6 (5s, 6C, CH-ar), 132.7 (C-ar), 134.2 (C-ar), 157.8 (C-3), 169.5, 169.7, 170.2, 170.5 (4s, O*C*OCH$_3$); MS (ESI) *m*/*z* = 513.9 [M+H]$^+$, 536.1 [M+Na]$^+$, 1026.7 [2M+H]$^+$, 1048.7 [2M+Na]$^+$; HRMS (ESI) *m*/*z* = $C_{26}H_{27}NO_{10}$Na [M+Na]$^+$ calcd 536.1533, found 536.1535.

4.2.7. (5*R*,7*R*,8*R*,9*S*,10*R*)-7-(Hydroxymethyl)-3-(4-methoxyphenyl)-1,6-dioxa-2-azaspiro[4,5]dec-2-ene-8,9,10-triol (4a)

A solution of **3a** (61 mg, 0.12 mmol) was treated according to method B. The residue was purified by flash silica gel column chromatography (PE/EtOAc, 3:2 then EtOAc then EtOAc/MeOH 9:1) to afford **4a** (40 mg, 98%) as a white solid. R_f = 0.34 (EtOAc/MeOH, 4:1); mp = 214–215 °C (MeOH/Et_2O); $[\alpha]_D^{20}$ = +105 (*c* 0.5, MeOH); ^{1}H NMR (500 MHz, CD_3OD, 55 °C, with CD_3OH as internal standard at 4.84 ppm) δ 3.60 (d, 1H, H-4a), 3.75 (dd, 1H, *J* = 8.9 Hz, *J* = 9.2 Hz, H-8), 3.89 (d, 1H, *J* = 9.8 Hz, H-10), 3.99–4.12 (m, 5H, H-4b CH_2OH H-7 H-9), 4.15 (s, 3H, OCH_3), 7.28 (d, 2H, *J* = 8.1 Hz, H-ar), 7.93 (d, 2H, *J* = 8.1 Hz, H-ar). The reported data[16] were referenced with CD_2HOD as internal standard at 3.31 ppm; ^{13}C NMR (125 MHz, CD_3OD, 55 °C) δ 44.6 (C-4), 56.0 (OCH_3), 62.6 (CH_2OH), 71.7 (C-8), 73.3 (C-10), 75.9 (C-9), 76.4 (C-7), 110.7 (C-5), 115.4 (s, 2C, CH-ar), 123.1 (C-ar), 129.5 (s, 2C, CH-ar), 159.5 (C-3), 163.2 (C-ar); MS (ESI) *m*/*z* = 326.0 [M+H]$^+$, 348.0 [M+Na]$^+$, 672.9 [2M+Na]$^+$, 997.6 [3M+Na]$^+$; HRMS (ESI) *m*/*z* = $C_{15}H_{20}N_1O_7$ [M+H]$^+$ calcd 326.1240, found 326.1243.

4.2.8. (5*R*,7*R*,8*R*,9*S*,10*R*)-7-(Hydroxymethyl)-3-(4-toluyl)-1,6-dioxa-2-azaspiro[4,5]dec-2-ene-8,9,10-triol (4b)

A solution of **3b** (135 mg, 0.30 mmol) was treated according to method B. The residue was purified by flash silica gel column chromatography (PE/EtOAc, 3:2 then EtOAc then EtOAc/MeOH 9:1) to afford **4b** (81 mg, 93%) as a pale yellow solid. R_f = 0.31 (EtOAc/MeOH, 9:1); mp = 200–202 °C; $[\alpha]_D^{20}$ = +73 (*c* 1, MeOH); ^{1}H NMR (300 MHz, CD_3OD, with CD_2HOD as internal standard at 3.31 ppm) δ 2.36 (s, 3H, PhCH_3), 3.44 (d, 1H, *J* = 17.6 Hz, H-4a), 3.44 (dd, 1H, *J* = 9.3 Hz, *J* = 9.5 Hz, H-8), 3.58 (d, 1H, *J* = 9.8 Hz, H-10), 3.67–3.85 (m, 5H, CH_2OH H-4b H-7 H-9), 7.24 (d, 2H, *J* = 8.1 Hz, H-ar), 7.56 (d, 2H, *J* = 8.1 Hz, H-ar); ^{13}C NMR (75 MHz, CD_3OD): δ 21.5 (PhCH_3), 44.3 (C-4), 62.4 (CH_2OH), 71.4 (C-8), 73.2 (C-10), 75.9 (C-7), 76.2 (C-9), 110.7 (C-5), 127.7 (C-ar), 127.8 (s, 2C, CH-ar), 123.6 (s, 2C, CH-ar), 141.2 (C-ar),159.6 (C-3); MS (ESI) *m*/*z* = 310.0 [M+H]$^+$, 332.0 [M+Na]$^+$, 640.9 [2M+Na]$^+$; HRMS (ESI) *m*/*z* = $C_{15}H_{20}NO_6$ [M+H]$^+$ calcd 310.1291 found 310.1292.

4.2.9. (5*R*,7*R*,8*R*,9*S*,10*R*)-7-(Hydroxymethyl)-3-(phenyl)-1,6-dioxa-2-azaspiro[4,5]dec-2-ene-8,9,10-triol (4c)

A solution of **3c** (17.6 mg, 0.04 mmol) was treated according to method B. The residue was purified by flash silica gel column chromatography (PE/EtOAc, 3:2 then EtOAc then EtOAc/MeOH 9:1) to afford **4c** (11 mg, 97%) as a pale yellow solid. R_f = 0.36 (EtOAc/MeOH, 4:1); mp = 195–197 °C (MeOH/Et_2O); $[\alpha]_D^{20}$ = +69 (*c* 0.63, MeOH); ^{1}H NMR (300 MHz, CD_3OD, with CD_2HOD as internal standard at 3.31 ppm) δ 3.35 (d, 1H, H-4a), 3.45 (t, 1H, *J* = 9.3 Hz, *J* = 10.0 Hz, H-8), 3.60 (d, 1H, *J* = 9.7 Hz, H-10), 3.69–3.77 (m, 4H, CH_2OH H-4b H-9), 3.83 (ddd, 1H, *J* = 2.3 Hz, *J* = 4.7, *J* = 10.0 Hz, H-7), 7.44 (m, 3H, H-ar), 7.69 (m, 2H, H-ar); ^{13}C NMR (75 MHz, CD_3OD) δ 44.2 (C-4), 62.4 (CH_2OH), 71.4 (C-8), 73.2 (C-10′), 75.9 (C-7), 76.2 (C-9), 110.9 (C-5), 127.8 (s, 2C, CH-ar), 129.9 (s, 2C, CH-ar), 130.6 (C-ar),131.6 (C-ar), 159.6 (C-3); MS (ESI) *m*/*z* = 296.0 [M+H]$^+$, 318.0 [M+Na]$^+$, 612.9 [2M+Na]$^+$; HRMS (ESI) *m*/*z* = $C_{14}H_{17}N_1O_6$Na [M+Na]$^+$ calcd 318.0954, found 318.0951.

4.2.10. (5*R*,7*R*,8*R*,9*S*,10*R*)-7-(Hydroxymethyl)-3-(4-nitrophenyl)-1,6-dioxa-2-azaspiro[4,5]dec-2-ene-8,9,10-triol (4d)

A solution of **3d** (51 mg, 0.10 mmol) was treated according to method B. The residue was purified by flash silica gel column chromatography (PE/EtOAc, 3:2 then EtOAc then EtOAc/MeOH 9:1) to afford **4d** (34 mg, 99%) as a pale yellow solid. R_f = 0.30 (EtOAc/MeOH, 4/1); mp = 181–182 °C (MeOH/Et_2O); $[\alpha]_D^{20}$ = +46 (*c* 0.5, MeOH); ^{1}H NMR (500 MHz, CD_3OD, 55 °C, with CD_3OH as internal standard at 4.84 ppm) δ 3.71 (d, 1H, H-4a), 3.81 (dd, 1H, *J* = 9.4 Hz, *J* = 9.6 Hz, H-8), 3.96 (d, 1H, *J* = 9.3 Hz, H-10), 4.05–4.12 (m, 3H, CH_2OH H-4b H-9), 4.14 (dd, 1H, *J* = 2.4 Hz, *J* = 12.0 Hz, CH_2OH), 4.19 (ddd, 1H, *J* = 9.6 Hz, *J* = 2.4 Hz, *J* = 4.8, H-7), 8.27 (d, 2H, *J* = 8.6 Hz, H-ar), 8.62 (d, 2H, *J* = 8.6 Hz, H-ar); ^{13}C NMR (125 MHz, CD_3OD, 55 °C) δ 43.8 (C-4), 62.6 (CH_2OH), 71.6 (C-8), 73.4 (C-10), 76.19, 76.21 (2s, 2C, C-7 C-9), 111.9 (C-5), 125.0 (s, 2C, CH-ar), 128.7 (s, 2C, CH-ar), 136.9 (C-ar), 150.3 (C-ar), 158.2 (C-3); MS (ESI) *m*/*z* = 341.0 [M+H]$^+$, 363.0 [M+Na]$^+$; HRMS (ESI) *m*/*z* = $C_{14}H_{17}N_2O_8$Na [M+H]$^+$ calcd 341.0985, found 341.0987.

4.2.11. (5*R*,7*R*,8*R*,9*S*,10*R*)-7-(Hydroxymethyl)-3-(2-naphthyl)-1,6-dioxa-2-azaspiro[4,5]dec-2-ene-8,9,10-triol (4e)

A solution of **3e** (130 mg, 0.25 mmol) was treated according to method B. The residue was purified by flash silica gel column chromatography (PE/EtOAc, 3:2 then EtOAc then EtOAc/MeOH 9:1) to afford **4e** (68 mg, 78%) as a white solid. R_f = 0.50 (EtOAc/MeOH 4:1); mp = 196–198 °C; $[\alpha]_D^{20}$ = +68 (*c* 0.33, MeOH); ^{1}H NMR (500 MHz, CD_3OD, 60 °C, with CD_2HOD as internal standard at 3.31 ppm) δ 3.46 (d, 1H, *J* = 17.4 Hz, H-4a), 3.47 (dd, 1H, *J* = 9.2 Hz, *J* = 9.7 Hz, H-8), 3.64 (d, 1H, *J* = 9.7 Hz, H-10), 3.71–3.88 (m, 5H, CH_2OH H-4b H-7 H-9), 7.53 (m, 2H, H-ar), 7.89 (m, 4H, H-ar), 8.05 (s, 1H, H-ar); ^{13}C NMR (125 MHz, CD_3OD, 60 °C) δ 44.3 (C-4), 62.7 (CH_2OH), 71.7 (C-8), 73.4 (C-10), 76.0 (C-7), 76.4 (C-9), 111.1 (C-5), 124.2, 127.9 (2s, 2C, CH-ar), 128.2 (C-ar), 128.4, 128.5, 128.9, 129.6 (4s, 5C, CH-ar), 134.7 (C-ar), 135.8 (C-ar), 159.8 (C-3); MS (ESI) *m*/*z* = 346 [M+H]$^+$, 712.9 [2M+Na]$^+$; HRMS (ESI) *m*/*z* = $C_{18}H_{20}NO_6$ [M+H]$^+$ calcd 346.1291, found 346.1291.

4.3. Enzyme kinetics

Rabbit muscle GPb was isolated, purified, recrystallized, and assayed as described.[53,54] Kinetic experiments were performed in the direction of glycogen synthesis in the presence of constant concentrations of glycogen (0.2% w/v), AMP (1 mM), various concentrations of Glc-1-P (2–20 mM) and inhibitors, in 30 mM imidazole buffer (pH 6.8), 60 mM KCl, 0.6 mM dithiothreitol, 0.6 mM EDTA, and 2% DMSO.[55]

4.4. X-ray crystallography

Native T-state GPb crystals, grown in the tetragonal lattice, space group $P4_32_12$,[56] were soaked with either 20 mM **4a** (for 10 h), 20 mM **4c** (for 5 h, or 20 mM **4d** (for 10 h) in a buffered solution (10 mM Bes, pH 6.7, 10–20% DMSO), prior data collection. Similarly, data for GPb–**4e** and GPb–**4b** complexes were collected from single crystals soaked with either 6 mM **4e** (for 5 h) or 30 mM **4b** in

10 mM Bes, pH 6.7, 30% DMSO, prior to mounting in a loop and flash-cooling in the nitrogen stream at 100 K. Diffraction data were collected from single crystals at EMBL-Hamburg outstation (Beamline X13) and SRS, Daresbury Laboratory (PX 9.6) at 293 K for **4a**, **4c**, and **4d** and 100 K for **4b** and **4e**. Data reduction and integration followed by scaling and merging of the intensities obtained was performed with Denzo and Scalepack, respectively, as implemented in HKL suite.[57]

Crystallographic refinement of the complexes was performed by maximum-likelihood methods using REFMAC.[42] The starting model employed for the refinement of the complex was the 100 K structure of the native T-state GPb determined at 2.0 Å resolution.[10] $2F_o - F_c$ and $F_o - F_c$ electron density maps were calculated and visualized using the program for molecular graphics 'O'.[58] Ligand models of **4a**–**e** compounds were fitted to the electron density maps after adjustment of their torsion angles. Alternate cycles of manual rebuilding with 'O' and refinement with REFMAC improved the quality of the models.

The stereochemistry of the protein residues was validated by PROCHECK.[59,60] Hydrogen bonds and van der Waals interactions were calculated with the program CONTACT as implemented in CCP4[59] applying a distance cut off 3.3 Å and 4.0 Å, respectively. Protein structures were superimposed using LSQKAB.[59] The figures were prepared with the program MOLSCRIPT[61] and rendered with Raster3D[62] and with the program MG.[63,64] Coordinate sets for comparisons were 2PYD (100 K GPb-α-D-glucose complex) or 100 K T-state native GPb (code 2GPN). The coordinates of the new structures have been deposited with the RCSB Protein Data Bank (http://www.rcsb.org/pdb) with codes 2QRG (GPb–**4a** complex), 2QRQ (GPb–**4b** complex), 2QRH (GPb–**4c** complex), 2QRM (GPb–**4d** complex), and 2QRP (GPb–**4e** complex).

4.5. Docking calculations

Docking calculations were performed using the program GLIDE 4.5.[51] The initial setup of the GPb enzyme for docking of the ligands was performed using Schrodingers' 'Protein Preparation Wizard', starting from the X-ray crystal structure of the GPb–**4e** complex. Residual DMSO molecules along with all crystallographic H_2O molecules were deleted, bond orders assigned and hydrogen atoms added. The initial assignments of protonation states for basic and acidic residues and tautomeric states was based on pK_a at their normal pH (7.0). However, subsequent optimization of hydroxyl, histidine protonation states and C/N atom 'flips', and sidechain O/N atom 'flips' of Asn and Gln was based on optimizing hydrogen bonding patterns, so that the final assignments were checked on visual inspection of the protein. In particular, all final His residues were assigned as neutral, either in a HIE or HID state. The phosphate in PLP was used in its mono-anion form. Finally, an 'Impref' minimization of the GPb–**4e** complex was performed using the OPLS-AA (2001) force field to remove steric clashes and bad contacts. At the end of the minimization, the root-mean-square deviation (RMSD) of all heavy atoms was within 0.3 Å of the crystallographic positions.

In the docking calculations with GLIDE, the shape and properties of the catalytic binding site were mapped onto grids with dimensions of 27 Å × 27 Å × 27 Å, centered on the **4e** ligand. The five ligands **4a**–**e** were extracted from their crystal complex structures and prepared for docking using Schrodingers' Maestro and the BUILD module, followed by minimization (500 steps, TNCG) using the OPLS-AA (2001) force field and MacroModel.[65] The minimized structures (500 steps, TNCG) were then subjected to a conformational search in bulk water solvent (GB/SA continuum model).[66–68] 1000 steps of the mixed mode Monte Carlo Multiple Minima/Low-Mode conformational search (MCMM/LMCS) algorithm were used.[69,70] Unique conformations (based on an RMSD of 0.5 Å for heavy atoms and O–H hydrogen atoms) within 100 kJ/mol of the global minimum conformation were saved for each ligand, and these conformations then clustered using XCluster[71] into five sets of conformations based on atomic coordinate RMS differences. The 'leading' or lowest energy conformation was taken from each of the five clusters. The resulting five conformations/ligand were then taken, plus the original minimized conformation for each ligand, and these six conformations were used for docking into the previously prepared **4e** receptor. Docking accuracy is limited by sampling so that use of an ensemble of conformations for each ligand will help reduce errors associated with inadequate sampling.

For the GLIDE docking runs, both the extra-precision (XP)[17,18] mode with standard OPLS-AA(2001) charges (standard GLIDE-XP) and quantum mechanics—polarized ligand docking (QPLD-XP) were performed.[20] In the GLIDE-XP docking runs, standard parameters were applied including van der Waals scaling for non-polar atoms (by 0.8) to include modest 'induced fit' effects, with up to 3 poses per ligand input conformation saved. For QPLD-XP docking runs, the output docking poses from GLIDE-XP docking with OPLS-AA(2001) partial charges were used to obtain electrostatic potential (ESP) fit ligand charges using the program QSITE[20] and the QM/MM method in the 'field' of the receptor, and for comparison, ESP fit ligand charges in the gas phase (free ligand; no receptor) using QM. Single point energy calculation using the B3LYP[72–74] density functional theory (DFT) method and 6–31G* basis sets[75–77] on the ligand (QM part) and the OPLS-AA forcefield for the receptor (MM part) were used for this purpose. The ligands were then redocked into the catalytic site using GLIDE in XP mode and the new ligand charges. Binding constraints on the glucopyranose were applied in the docking calculations as described in Section 2.4 and Tables 1 and 2. The obtained ligand poses were considered conformationally distinct if their RMSD (heavy atoms) was larger than 0.5 Å. The quality of the docking results was assessed by comparing (superimposing) the top-ranked pose for each method with the native X-ray conformation from the GPb–ligand complexes, and measurement of the correlation between the GlideScores obtained and experimental binding free energies. Docked ligand binding conformation results were considered 'accurate' when the RMSD of the ligand heavy atom positions in the top-ranked pose and the crystallographic conformation was less than 1.0 Å.

Breakdown of the contributions to GlideScores using the XP-Visualizer module was performed for the most successful docking method (QPLD-XP, ESP fit charges calculated in receptor 'field', and constraints on the glucopyranose moiety positions). This allowed us to analyze and compare the contributions of the different descriptor terms for the individual ligands.

Acknowledgements

This work was supported by the EU Marie Curie Early Stage Training (EST) contract no MEST-CT-020575; a Marie Curie Host Fellowships for the Transfer of Knowledge (ToK) contract no MTKD-CT-2006-042776; the Greek GSRT Scientific and Technological cooperation between Greece and USA (2004–2007); the Hellenic General Secretariat for Research and Technology (GSRT), Ministry of Development, through the program 'Excellence in Research Institutes (2nd cycle)' to N.G.O.; the EMBL-Hamburg outstation under FP6 'Structuring the European Research Area Programme' contract no RII3/CT/2004/5060008, and SRS Daresbury Laboratory (contract IHPP HPRI-CT-1999-00012). Financial support by University Lyon 1, CNRS, the Région Rhône-Alpes (funds from MIRA Recherche 2001 & 2006 and stipends to M.B.) and the European Union (FP6-IP 503467) is gratefully acknowledged. Support provided by the French Ministry of Foreign Affairs (PAI Balaton

n°11 061PE) is also acknowledged. We would furthermore like to thank Schrödinger, particularly Jianxin Duan for technical support and useful discussions regarding the computational work.

Supplementary data

Supplementary data (data collection and refinement statistics for compounds **4a**–**e**, hydrogen bonding interactions, water hydrogen-bonding network and Van der Waals interactions for compound **4a**–**e**) associated with this article can be found, in the online version, at doi:10.1016/j.bmc.2009.08.060.

References and notes

1. Ross, S. A.; Gulve, E. A.; Wang, M. H. *Chem. Rev.* **2004**, *104*, 1255.
2. American Diabetes Association. *Diabetes Care* **2004**, *27*, S5.
3. Baker, D. J.; Timmons, J. A.; Greenhaff, P. L. *Diabetes* **2005**, *54*, 2453.
4. Lukacs, C. M.; Oikonomakos, N. G.; Crowther, R. L.; Hong, L. N.; Kammlott, R. U.; Levin, W.; Li, S.; Liu, C. M.; Lucas-McGady, D.; Pietranico, S.; Reik, L. *Prot. Struct. Funct. Bioinf.* **2006**, *63*, 1123.
5. Treadway, J. L.; Mendys, P.; Hoover, D. J. *Exp. Opin. Invest. Drugs* **2001**, *10*, 439.
6. Oikonomakos, N. G.; Somsak, L. *Curr. Opin. Invest. Drugs* **2008**, *9*, 379.
7. Somsák, L.; Czifrák, K.; Tóth, M.; Bokor, É.; Chrysina, E. D.; Alexacou, K.-M.; Hayes, J. M.; Tiraidis, C.; Lazoura, E.; Leonidas, D. D.; Zographos, S. E.; Oikonomakos, N. G. *Curr. Med. Chem.* **2008**, 2933.
8. Baker, D. J.; Greenhaff, P. L.; Timmons, J. A. *Exp. Opin. Ther. Patents* **2006**, *16*, 459.
9. Henke, B. R.; Sparks, S. M. *Mini-Rev. Med. Chem.* **2006**, *6*, 845.
10. Gregoriou, M.; Noble, M. E. M.; Watson, K. A.; Garman, E. F.; Krulle, T. M.; De-La-Fuente, C.; Fleet, G. W. J.; Oikonomakos, N. G.; Johnson, L. N. *Protein Sci.* **1998**, *7*, 915.
11. Martin, J. L.; Veluraja, K.; Ross, K.; Johnson, L. N.; Fleet, G. W. J.; Ramsden, N. G.; Bruce, I.; Orchard, M. G.; Oikonomakos, N. G.; Papageorgiou, A. C.; Leonidas, D. D.; Tsitoura, H. S. *Biochemistry* **1991**, *30*, 10101.
12. Praly, J.-. P.; Boye, S.; Joseph, B.; Rollin, P. *Tetrahedron Lett.* **1993**, *34*, 3419.
13. Elek, R.; Kiss, L.; Praly, J.-. P.; Somsak, L. *Carbohydr. Res.* **2005**, *340*, 1397.
14. Somsák, L.; Nagy, V.; Vidal, S.; Czifrák, K.; Berzsényi, E.; Praly, J.-. P. *Bioorg. Med. Chem. Lett.* **2008**, *18*, 5680.
15. Nagy, V.; Benltifa, M.; Vidal, S.; Berzsényi, E.; Teilhet, C.; Czifrák, K.; Batta, G.; Docsa, T.; Gergely, P.; Somsák, L.; Praly, J.-. P. *Bioorg. Med. Chem.* **2009**, *17*, 5696.
16. Benltifa, M.; Vidal, S.; Gueyrard, D.; Goekjian, P. G.; Msaddek, M.; Praly, J.-. P. *Tetrahedron Lett.* **2006**, *47*, 6143.
17. Friesner, R. A.; Banks, J. L.; Murphy, R. B.; Halgren, T. A.; Klicic, J. J.; Mainz, D. T.; Repasky, M. P.; Knoll, E. H.; Shelley, M.; Perry, J. K.; Shaw, D. E.; Francis, P.; Shenkin, P. S. *J. Med. Chem.* **2004**, *47*, 1739.
18. Friesner, R. A.; Murphy, R. B.; Repasky, M. P.; Frye, L. L.; Greenwood, J. R.; Halgren, T. A.; Sanschagrin, P. C.; Mainz, D. T. *J. Med. Chem.* **2006**, *49*, 6177.
19. Alexacou, K. M.; Hayes, J. M.; Tiraidis, C.; Zographos, S. E.; Leonidas, D. D.; Chrysina, E. D.; Archontis, G.; Oikonomakos, N. G.; Paul, J. V.; Varghese, B.; Loganathan, D. *Prot. Struct. Funct. Bioinf.* **2008**, *71*, 1307.
20. Schrödinger Suite 2008 QM-Polarized Ligand Docking protocol; GLIDE Version 4.5, Schrödinger, LLC, New York, NY, 2007; JAGUAR Version 7.5, Schrödinger, LLC, New York, NY, 2008; QSITE Version 5.0, Schrödinger, LLC, New York, NY, 2008.
21. Cho, A. E.; Guallar, V.; Berne, B. J.; Friesner, R. *J. Comput. Chem.* **2005**, *26*, 915.
22. Raha, K.; Peters, M. B.; Wang, B.; Yu, N.; WollaCott, A. M.; Westerhoff, L. M.; Merz, K. M. *Drug Discovery Today* **2007**, *12*, 725.
23. Jorgensen, W. L.; Maxwell, D. S.; TiradoRives, J. *J. Am. Chem. Soc.* **1996**, *118*, 11225.
24. Klebe, G. *Drug Discovery Today* **2006**, *11*, 580.
25. Velec, H. F. G.; Gohlke, H.; Klebe, G. *J. Med. Chem.* **2005**, *48*, 6296.
26. Zeragraf, M.; Steuber, H.; Koch, C.; La Motta, C.; Sartini, S.; Sotriffer, C. A.; Klebe, G. *Angew. Chem., Int. Ed.* **2007**, *46*, 3575.
27. *1,3-Dipolar Cycloaddition Chemistry*; Padwa, A., Ed.; Wiley: New York, 1984.
28. *Cycloaddition Reactions in Carbohydrate Chemistry*; Giuliano, R. M., Ed.; American Chemical Society: Washington, DC, 1992.
29. Santoyo-Gonzalez, F.; Hernandez-Mateo, F. *Top. Heterocycl. Chem.* **2007**, *7*, 133.
30. Fernandez-Bolanos, J. G.; Lopez, O. *Top. Heterocycl. Chem.* **2007**, *7*, 31.
31. Gyorgydeak, Z.; Thiem, J.; Horton, D. *Adv. Carbohydr. Chem. Biochem.* **2006**, *60*, 103.
32. Pellissier, H. *Tetrahedron* **2007**, *63*, 3235.
33. Li, X.; Wang, R.; Wang, Y.; Chen, H.; Li, Z.; Ba, C.; Zhang, J. *Tetrahedron* **2008**, *64*, 9911.
34. Taillefumier, C.; Chapleur, Y. *Chem. Rev.* **2004**, *104*, 263.
35. Rajanbabu, T. V.; Reddy, G. S. *J. Org. Chem.* **1986**, *51*, 5458.
36. Bourdon, B.; Corbet, M.; Fontaine, P.; Goekjian, P. G.; Gueyrard, D. *Tetrahedron Lett.* **2008**, *49*, 747.
37. Gueyrard, D.; Haddoub, R.; Salem, A.; Bacar, N. S.; Goekjian, P. G. *Synlett* **2005**, 520.
38. Toth, M.; Kover, K. E.; Benyei, A.; Somsak, L. *Org. Biomol. Chem.* **2003**, *1*, 4039.
39. Toth, M.; Somsak, L. *J. Chem. Soc., Perkin Trans. 1* **2001**, 942.
40. Benltifa, M.; Vidal, S.; Fenet, B.; Msaddek, M.; Goekjian, P. G.; Praly, J.-P.; Brunyánszki, A.; Docsa, T.; Gergely, P. *Eur. J. Org. Chem.* **2006**, 4242.
41. Tóth, M.; Kun, S.; Bokor, É.; Benltifa, M.; Tallec, G.; Vidal, S.; Docsa, T.; Gergely, P.; Somsák, L.; Praly, J.-P. *Bioorg. Med. Chem.* **2009**, *17*, 4773.
42. Murshudov, G. N.; Vagin, A. A.; Dodson, E. J. *Acta Crystallogr., Sect. D* **1997**, *53*, 240.
43. Oikonomakos, N. G. *Curr. Prot. Pept. Sci.* **2002**, *3*, 561.
44. Chrysina, E. D.; Kosmopoulou, M. N.; Kardakaris, R.; Bischler, N.; Leonidas, D. D.; Kannan, T.; Loganathan, D.; Oikonomakos, N. G. *Bioorg. Med. Chem.* **2005**, *13*, 765.
45. Tsitsanou, K. E.; Oikonomakos, N. G.; Zographos, S. E.; Skamnaki, V. T.; Gregoriou, M.; Watson, K. A.; Johnson, L. N.; Fleet, G. W. J. *Protein Sci.* **1999**, *8*, 741.
46. Mitchell, E. P.; Withers, S. G.; Ermert, P.; Vasella, A. T.; Garman, E. F.; Oikonomakos, N. G.; Johnson, L. N. *Biochemistry* **1996**, *35*, 7341.
47. Zographos, S. E.; Oikonomakos, N. G.; Tsitsanou, K. E.; Leonidas, D. D.; Chrysina, E. D.; Skamnaki, V. T.; Bischoff, H.; Goldmann, S.; Watson, K. A.; Johnson, L. N. *Structure* **1997**, *5*, 1413.
48. Oikonomakos, N. G.; Tsitsanou, K. E.; Zographos, S. E.; Skamnaki, V. T.; Goldmann, S.; Bischoff, H. *Protein Sci.* **1999**, *8*, 1930.
49. Leonidas, D. D.; Zographos, S. E.; Oikonomakos, N. G., unpublished results.
50. Eldridge, M. D.; Murray, C. W.; Auton, T. R.; Paolini, G. V.; Mee, R. P. *J. Comput. Aided Mol. Des.* **1997**, *11*, 425.
51. GLIDE Version 4.5, User Manual, Schrödinger, LLC, New York, NY, 2007.
52. Archontis, G.; Watson, K. A.; Xie, Q.; Andreou, G.; Chrysina, E. D.; Zographos, S. E.; Oikonomakos, N. G.; Karplus, M. *Prot. Struct. Funct. Bioinf.* **2005**, *61*, 984.
53. Melpidou, A. E.; Oikonomakos, N. G. *FEBS Lett.* **1983**, *154*, 105.
54. Oikonomakos, N. G.; Zographos, S. E.; Johnson, L. N.; Papageorgiou, A. C.; Acharya, K. R. *J. Mol. Biol.* **1995**, *254*, 900.
55. Anagnostou, E.; Kosmopoulou, M. N.; Chrysina, E. D.; Leonidas, D. D.; Hadjiloi, T.; Tiraidis, C.; Zographos, S. E.; Gyorgydeak, Z.; Somsak, L.; Docsa, T.; Gergely, P.; Kolisis, F. N.; Oikonomakos, N. G. *Bioorg. Med. Chem.* **2006**, *14*, 181.
56. Oikonomakos, N. G.; Melpidou, A. E.; Johnson, L. N. *Biochim. Biophys. Acta* **1985**, *832*, 248.
57. Otwinowski, Z.; Minor, W. In *Macromolecular Crystallography, Pt A*, 1997; Vol. 276, p 307.
58. Jones, T. A.; Zou, J. Y.; Cowan, S. W.; Kjeldgaard, M. *Phys. Rev. B* **1991**, *47*, 110.
59. CCP4. *Acta Crystallogr., Sect. D* **1994**, *50*, 760.
60. Laskowski, R. A.; Macarthur, M. W.; Moss, D. S.; Thornton, J. M. *J. Appl. Crystallogr.* **1993**, *26*, 283.
61. Kraulis, P. *J. Appl. Crystallogr.* **1991**, *24*, 946.
62. Merritt, E. A.; Bacon, D. J.. In *Macromolecular Crystallography, Pt B*; Academic Press: San Diego, 1997; Vol. 277, p 505.
63. Potterton, E.; McNicholas, S.; Krissinel, E.; Cowtan, K.; Noble, M. *Acta Crystallogr., Sect. D* **2002**, *58*, 1955.
64. Potterton, L.; McNicholas, S.; Krissinel, E.; Gruber, J.; Cowtan, K.; Emsley, P.; Murshudov, G. N.; Cohen, S.; Perrakis, A.; Noble, M. *Acta Crystallogr., Sect. D* **2004**, *60*, 2288.
65. MacroModel, Version 9.5, Schrödinger, LLC, New York, NY, 2007.
66. Gallicchio, E.; Zhang, L. Y.; Levy, R. M. *J. Comput. Chem.* **2002**, *23*, 517.
67. Guvench, O.; Shenkin, P.; Kolossvary, I.; Still, W. C. *J. Comput. Chem.* **2002**, *23*, 214.
68. Still, W. C.; Tempczyk, A.; Hawley, R. C.; Hendrickson, T. *J. Am. Chem. Soc.* **1990**, *112*, 6127.
69. Chang, G.; Guida, W. C.; Still, W. C. *J. Am. Chem. Soc.* **1989**, *111*, 4379.
70. Kolossvary, I.; Guida, W. C. *J. Am. Chem. Soc.* **1996**, *118*, 5011.
71. MacroModel XCluster, Version 9.5, Schrödinger, LLC, New York, NY, 2005.
72. Becke, A. D. *J. Chem. Phys.* **1993**, *98*, 5648.
73. Lee, C. T.; Yang, W. T.; Parr, R. G. *Phys. Rev. B* **1988**, *37*, 785.
74. Stephens, P. J.; Devlin, F. J.; Chabalowski, C. F.; Frisch, M. J. *J. Phys. Chem.* **1994**, *98*, 11623.
75. Francl, M. M.; Pietro, W. J.; Hehre, W. J.; Binkley, J. S.; Gordon, M. S.; Defrees, D. J.; Pople, J. A. *J. Chem. Phys.* **1982**, *77*, 3654.
76. Hariharan, P. C.; Pople, J. A. *Theor. Chim. Acta* **1973**, *28*, 213.
77. Hehre, W.; Ditchfield, R.; Pople, J. A. *J. Chem. Phys.* **1972**, *56*, 2257.